SMART ADAPTIVE BEAM-FORMING ANTENNA DESIGN FOR NEXT GENERATION COMMUNICATION SYSTEMS

by

Ahmed Umar Kausar

A dissertation

submitted in partial fulfillment

of the requirements for the degree of

Doctor of Philosophy in Electrical and Computer Engineering

Boise State University

August 2018

BOISE STATE UNIVERSITY GRADUATE COLLEGE

DEFENSE COMMITTEE AND FINAL READING APPROVALS

of the dissertation submitted by

Ahmed Umar Kausar

Dissertation Title: Smart Adaptive Beam-Forming Antenna Design for Next Generation Communication Systems

Date of Final Oral Examination: 15 June 2018

The following individuals read and discussed the dissertation submitted by student Ahmed Umar Kausar, and they evaluated his presentation and response to questions during the final oral examination. They found that the student passed the final oral examination.

Dr. Hani Mehrpouyan, Ph.D.	Chair, Supervisory Committee
Dr. Nader Rafla, Ph.D.	Member, Supervisory Committee
Dr. Hao Chen, Ph.D.	Member, Supervisory Committee

The final reading approval of the dissertation was granted by Dr. Hani Mehrpouyan, Ph.D., Chair, Supervisory Committee. The dissertation was approved by the Graduate College.

Dedicated to my family and supervisor

ACKNOWLEDGMENTS

Boise is my second home, I have learned a lot during my stay at Boise State University. Before joining Boise State University, I had completed my masters from National University of Sciences and Technology (NUST), Pakistan and I had five years of work experience. Since my first day at Boise State University, Dr. Hani Mehrpouyan has been a source of great inspiration for me. I joined BSU three weeks after the start date of the fall 2015 semester, but with the kind support of my supervisor, I was able to adjust well to the new environment. I am deeply impressed by the work ethic and professionalism of Dr. Hani. He will always be my mentor.

Dr. Hani Mehrpouyan helped me understand advancements in millimeter-wave (mm-Wave) technology. Without the support of Dr. Hani, I would not have been able to accomplish my research goals. In Dr. Hani, I have found a person with the highest level of professionalism and a kind heart. Along with his research, Dr. Hani has also inspired me with his towering personality and gratitude. I am fortunate to be his student.

I am also incredibly thankful to Dr. Nader Nafla and the ECE department at Boise State University for providing me with an extremely favorable environment for research and assisting me in my first patent. I am also thankful to Muhammad Kamran Latif, Ruhollah Amiri and Luka Dawood for helping and assisting me during my research. Muhammad Kamran Latif was always there to help. He also provided me with great emotional and logistic support during my time at Boise. I am thankful to Dr. Hao Chen, Dr. Jim Browning, Dr. Kurtis Cantley, Dr. Bob Hay and Dr.

John Chaisson for teaching me courses that were fruitful during my research.

I will also like to thank Dr. James Peterson and Kenneth Peluso. They provided me with a perfect platform to accomplish my research objectives.

Last but not least, I am grateful to my family back home and here in the United States for their support.

ABSTRACT

Adaptive beamforming antennas open a new venue for research to achieve high data rates. Such antennas are of interest at higher frequencies, especially at millimeter-waves. Millimeter-wave band ranges from 30 GHz - 300 GHz. There is an ample bandwidth available in this spectrum. However, due to the significant path loss at high frequencies, there is a need for better error correction schemes and adaptive beam-forming antennas for this frequency band.

The goal of our research is to design a novel adaptive beamforming smart antenna that is low cost, compact, power-efficient and less complex. Based on our recently awarded US patent, we have devised a novel beamforming technique in which phased array and parasitic array approaches are used in conjunction with each other. Conventionally, phased array or switched array techniques are used in smart antennas for beam-steering. In phased array antennas each antenna element has a separate excitation. Therefore, such antennas are costly and impractical for use in everyday communication devices. Switched array antennas are cost-effective and simple to implement, but the antenna beam can only be formed at a predefined location.

Our proposed novel beamforming technique is based on a mathematical model. After mathematical modeling, the antenna is simulated in Ansoft High Frequency Structure Simulator (HFSS). Results of the simulated model in Ansoft HFSS and the mathematical model are in close agreement with each other, Ansoft HFSS uses the finite element method (FEM) for complex electromagnetic computations. Antenna design consists of two circular arrays of six parasitic elements. Each array has an

active element in its center and there is a fixed phase difference between excitation currents to the active elements. The beam is steered either by changing the phase difference between excitation currents to the active elements or by changing reactance of the parasitic elements. Our technique is novel as this is the first time switched parasitic array and phased array approaches are efficiently used in conjunction with each other. After mathematical modeling and simulations, two antennas are designed and tested. The first antenna is centered at 2.5 GHz. This antenna is used for proof of concept. The second antenna is centered at 28 GHz. The 28 GHz band will play a key role in the next generation of wireless networks, i.e., 5G. The antenna hardware testing results are also in line with the mathematical and the simulated models. This dissertation aims to provide an overview of smart adaptive beamforming antenna design, propose a mathematical model for novel hybrid beamforming, present the application of the proposed antenna in satellite communication and airborne communication, and demonstrate the validity of the design via software simulations and hardware testing.

TABLE OF CONTENTS

LIST OF TABLES

LIST OF FIGURES

LIST OF ABBREVIATIONS

– ESPAR Electronically Steerable Parasitic Array Radiator

– BER Bit Error Rate

– SNR Signal to Noise Ratio

– SINR Signal to Interference Noise Ratio

– FPGA Field Programmable Gate Array

– G/T Antenna Gain-to-Noise-Temperature

– mmWave Millimetric Waves

– EIRP Equivalent Isotropically Radiated Power

– GEO Geostationary Equatorial Orbit

– MEO Medium Earth orbit

– LEO Low Earth orbit

– BUC Block Up Converter

– LNB Low Noise Block

– COTP Communication on the Pause

– COTM Communication on the Move

– QPSK Quadrature Phase Shift Keying

– BTS Base Transceiver Station

– FEM Finite Element Method

– DSP Digital Signal Processing

CHAPTER 1

INTRODUCTION

1.1 Introduction

In the last few decades, there is an ever-increasing demand for higher data rates and improved spectral efficiency. The current frequency spectrum is depleting, and it has become a precious commodity [1]. Advancements in digital signal processing (DSP) have pushed channel capacity close to its theoretical limits as defined by Shanon's equation. To further increase data rates and spectral efficiency in wireless communications, smart antennas have become a topic of active research. Smart antennas have adaptive beamforming capability and the beam is formed in accordance with the environment. By using a smart antenna, nulls can be placed in the direction of the interfering signals. Signal to interference noise ratio (SINR) can be greatly improved by using smart antennas. As of today, smart antennas are not used in everyday communication devices due to the complexity of design and cost. Traditionally, the phased array approach or the switched array approach is used in smart antennas. Most of the smart antennas in the market are phased array antennas. Such antennas require excitation and a phase shifter at each element. Therefore, the cost of implementation and complexity is high. As a result, phased array antennas are only used in high-end devices. Switched array antennas provide a simple and low-cost solution for beam-steering, but the beam can only be formed in a predefined

direction.

Harrington introduced the concept of parasitic array antennas for commercial application of smart antennas [2]. Parasitic array antennas exploit mutual coupling between antenna elements. Therefore, the size of such antennas is smaller as compared to the phased array antennas. Parasitic array antennas have an array of passive elements and an active element. Each parasitic element is loaded with a varactor diode. The antenna beam is steered by changing the reactance of the passive elements. Parasitic array antennas have the following advantages:

- In parasitic array antennas, antenna elements can be placed closer than 0.5 $\times\lambda$ to each other, where λ is the wavelength. As a result, such antennas are compact.

- Phase shifters are not used in parasitic array antennas. Each element is loaded by a varactor. By varying reactance of the passive elements, the beam is steered. Since the proposed design does not include phase shifters, parasitic array antennas are cost-effective and the design is less complex as compared to phased array technology.

Equivalent isotropically radiated power (EIRP) is obtained by multiplying the gain of the transmit antenna (G_t) with the transmit antenna power (P_t) [3]. The formula for EIRP is:

$$EIRP = P_t \times G_t \tag{1.1}$$

From above, we can note that by using a directional antenna instead of an isotropic antenna, G_t increases, which in turn increases equivalent isotropically radiated power (EIRP). The millimeter-wave (mm-Wave) band is considered as a potential solution

for next-generation communication systems. The mm-Wave signals have higher path loss. In order to cater for high propagation loss, instead of omnidirectional antennas, adaptive beamforming smart antennas are to be used for next-generation mm-Wave networks. Smart antennas are a way forward for designing an efficient and reliable wireless communication network.

Due to the demand for high data rates in 5G and scarcity of available bandwidth at lower frequencies, the FCC has opened 10.85 GHz of spectrum for potential 5G applications in the frequency ranges beyond 24 GHz. The following bands are specifically made available for this application:

- 27.5 GHz - 28.35 GHz (0.85 GHz bandwidth)
- 37GHz - 40 GHz (3 GHz bandwidth)
- 64-71 GHz (7 GHz)

Major cellular service providers in the USA (T-Mobile, Verizon, and AT&T) have started testing 5G in the 28 GHz spectrum. The bands in the 27.5 GHz - 38.35 GHz and the 37 GHz - 40 GHz frequency range are licensed bands, whereas the 64 GHz - 71 GHz band is allocated for the unlicensed use. The 64 GHz - 71 GHz band is adjacent to the ISM band from 57 GHz - 64 GHz [4]. We have designed two antennas: one antenna is designed at 2.5 GHz and the other antenna is designed at 28 GHz. The 2.5 GHz antenna is used as a prototype for proof of concept of our proposed novel hybrid beamforming technique. The 28 GHz antenna is designed for the potential integration with 5G terminals. We have selected 28 GHz as our center frequency because the 27.5 GHz- 28.35 GHz band has received significant attention as a potential band for 5G rollout.

1.2 Back Ground

An antenna is basically a transducer that converts radio frequency (RF) into alternating current (AC) and vice versa. The antenna is an integral part of communication systems. It is important to note that an antenna is a passive device. Smart antennas are an important class of antennas. These antennas use signal processing techniques in order to form maxima in a given direction. The beams of the smart antennas can be steered by the following two mechanisms:

- Mechanical beam steering
- Electronic beam steering

1.2.1 Mechanical Beamsteering

In mechanical beam steering, the antenna beam is mechanically steered. Mechanical beam-steering involves physically moving the antenna in an intended direction. Mechanical beam-steering is not a preferred method due to the following reasons [5, 6]:

- It involves wear and tear of the moving parts, especially motors.
- It requires relatively higher power consumption levels because motors have to move the antenna physically.
- Mechanical beam-steering is slow in comparison to electronic beam-steering.
- Such antennas are susceptible to the mechanical issues due to the presence of the moving parts.

1.2.2 Electronic Beamsteering

Electronic Beam-steering does not include moving parts and the antenna radiation pattern is electronically steered. Electronic beam-steering is the preferred approach for smart antenna design because it does not involve moving parts and this approach is more robust as compared to that of mechanical beam-steering. Electronic steering methods are outlined in the subsections below:

1.2.2.1 Analog, Digital and Hybrid Beamforming

The above techniques involve combining the signals of each antenna element in an array such that a directional beam is formed in the intended direction. There is constructive interference in the desired direction and destructive interference in the direction of the interfering source. Electronic beam-steering can be categorized as:

- Analog beamforming
- Digital beamforming
- Hybrid beamforming

In analog beam-forming, each antenna element in an antenna array is fed through a phase shifter. The beam is steered by controlling the individual phase of the antenna elements [7]. Fig. 1.1 shows the conceptual implementation of the approach. Analog beamforming is easy to implement and it has less power consumption as compared to the digital beamforming. However, at higher frequencies, specifically at 28 GHz and beyond, the bandwidth of the phase shifters can pose limitations for the operations of the antenna. Analog beamforming is mainly used in phased array antennas. Since the design requires phase shifters, this approach is expensive to implement. Moreover,

each antenna element has to be separated by at least 0.7 x λ from the other elements. As a result, phased array antennas cannot be designed in a compact package. Given their high costs phased array antennas are only used in specialized devices [8]. Phase shifters can be analog or digital. In the case of analog phase shifters, the phase is varied by varying the voltage across the phase shifter. Analog phase shifters provide a continuous phase shift, but such phase shifters are prone to external noise which may cause inaccurate results. On the other hand, digital phase shifters result in discrete phase shifts and are, subsequently, less prone to external noise.

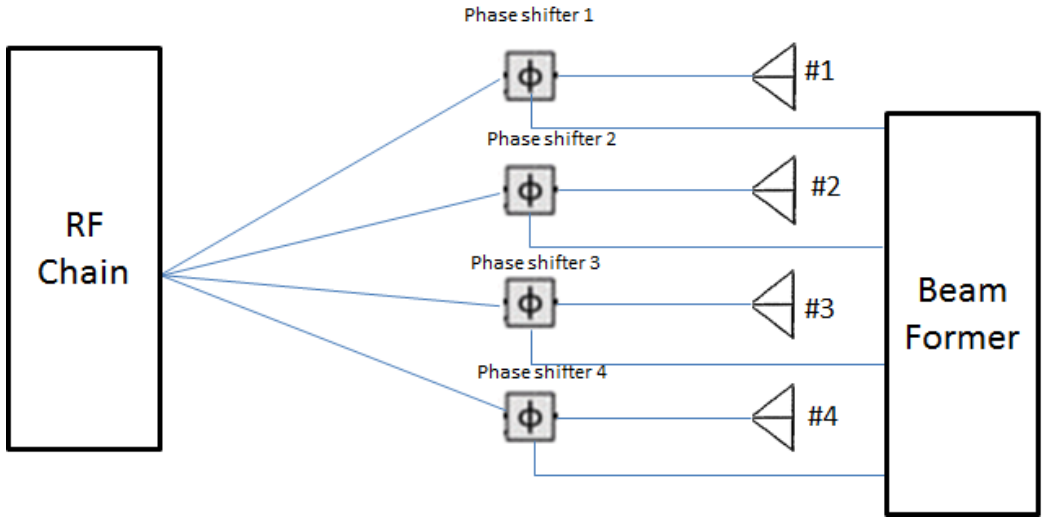

Figure 1.1: Phased array antenna

In digital beamforming, digital signal processing is used for varying the phase shift between antenna elements. This technique requires multiple RF chains as shown in Fig. 1.2. A signal is first converted into the digital form, and after that, the base-band signal is fed to the beamforming algorithm through a channelizer [9]. Beamforming algorithms adjust phase shift such that the antenna beam can be steered in any desired direction. Digital beamforming is complex and power hungry due to the presence of a large number of RF chains.

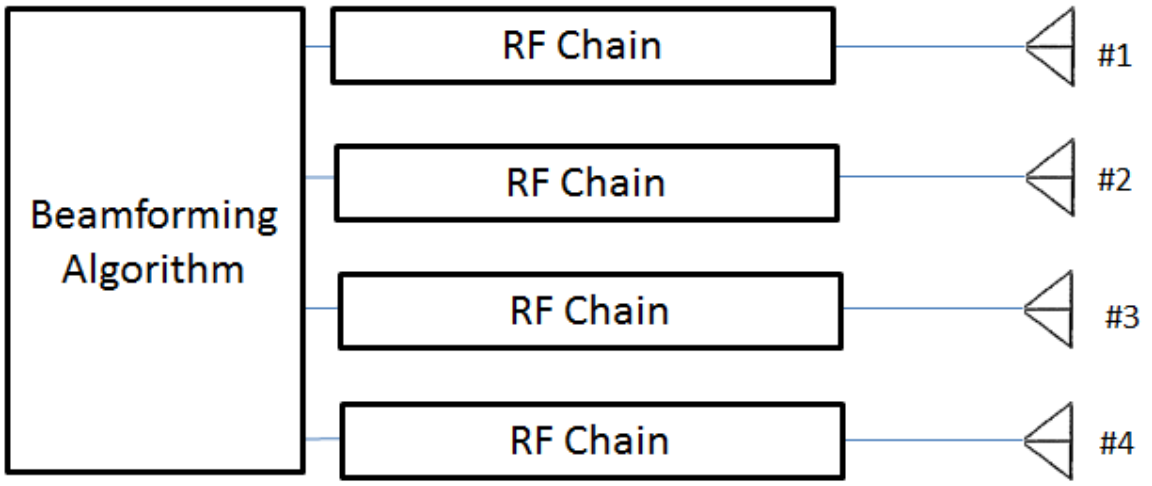

Figure 1.2: Digital Beamforming

A hybrid beamformer is a combination of analog beamforming and digital beamforming. Fig. 1.3 shows a block diagram for the hybrid beamforming. Hybrid beamforming requires a fewer number of RF chains [10].

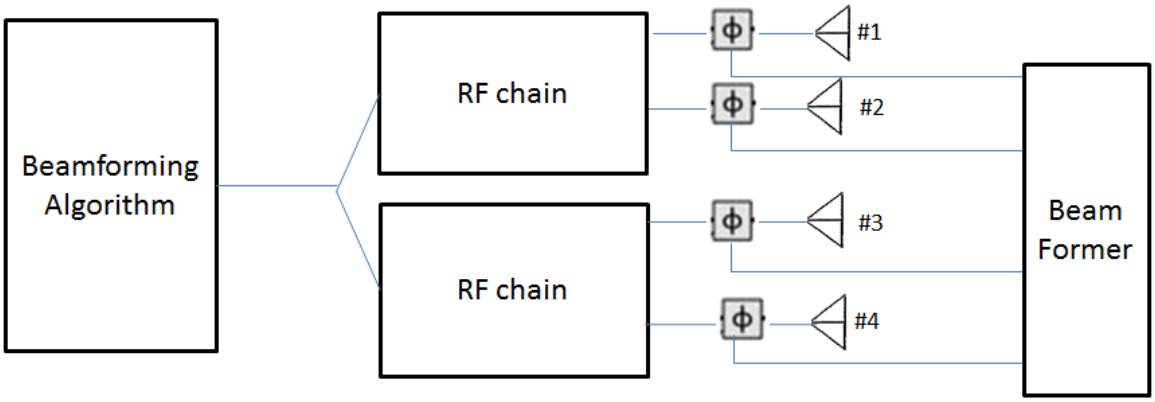

Figure 1.3: Hybrid Beamforming

1.2.2.2 Switched Array Antennas

In switched array antennas, there are multiple directional antennas in an array and the feed element is connected to one of these antennas at any given time. For

beam-switching, the feed is switched from one antenna to another. Fig. 1.4 shows a switched array antenna. Here, the beam can be steered in one of the four directions by activating the antenna situated in the desired beam direction. A switched array has redundant antennas. As a result, the cost of implementation may be high [11].

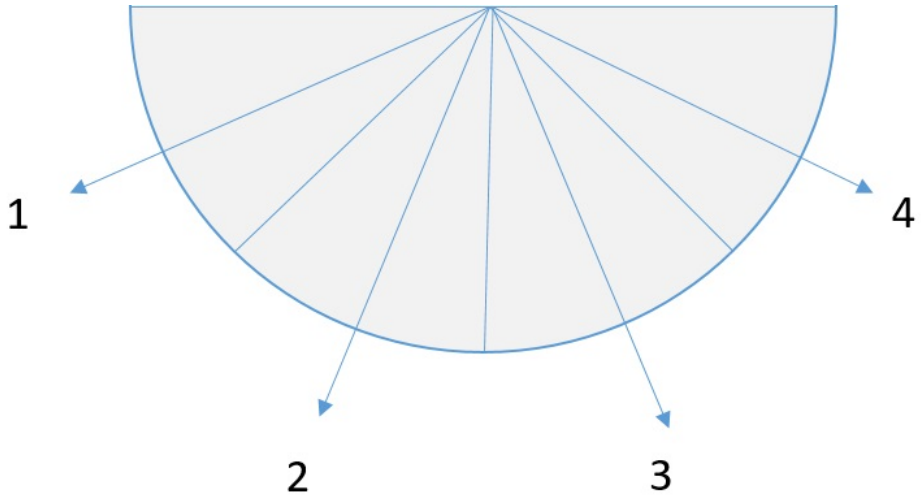

Figure 1.4: Switched Array Antenna

1.2.2.3 Lens Antennas

In lens antennas, an elliptical lens of dielectric material is placed at the focal length of an antenna array. Fig. 1.5 shows a lens antenna, where each element is placed at a distance L from another element. Elements are positioned such that the radiation of each element is directed from the focal point of the lens. Only one antenna is activated at a time by using control switches. Lens antennas are highly directional and yield a high gain [12]. The lens antenna design does not include phase shifters. Therefore, the cost of implementation is low [13]. A shortcoming of the lens antenna is that the beam can be formed only at predefined locations.

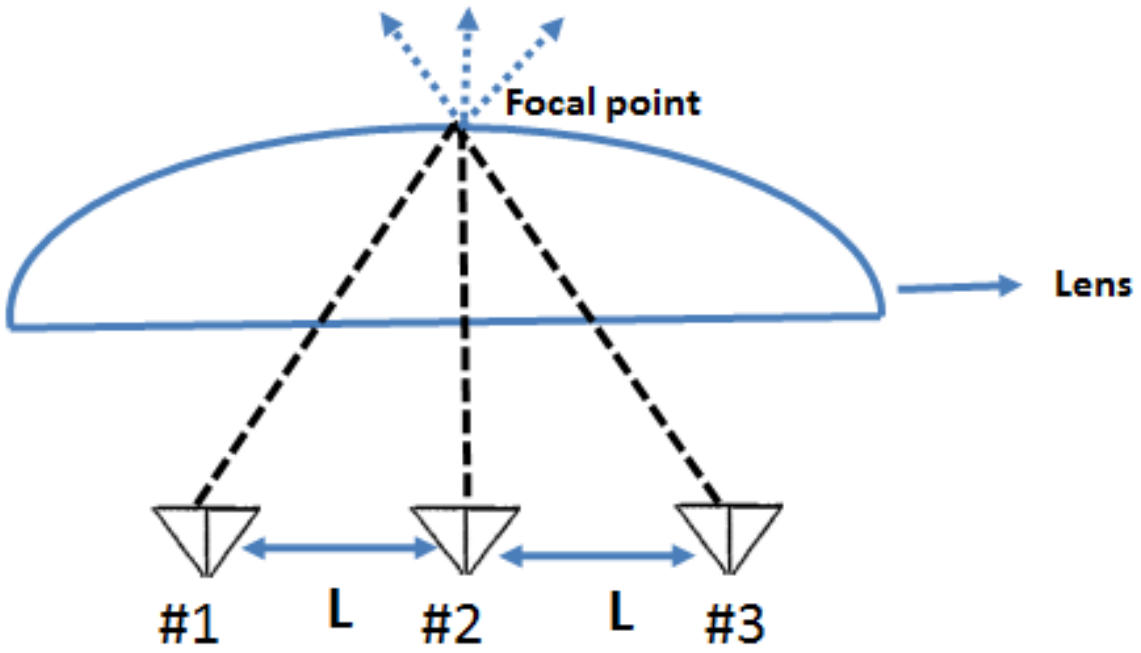

Figure 1.5: Lens Antenna

1.2.2.4 Reflectarray Antennas

Reflectarray antennas use a hybrid of parabolic antennas and array antennas. The feed of reflectarray antennas is the same as that of a parabolic antenna. However, instead of a single parabolic reflector, there are multiple reflector elements which reflect the incident signal from the feed. Reflectors can either be active (phase shifters) or passive (phase is varied by changing the size of the element). The phase shift between antenna elements regulates beam-steering. Unlike parabolic antennas, reflectarray antennas do not require motors for steering antenna radiation patterns [14, 15]. Due to the presence of phase shifters, reflectarray antennas are costly. Fig. 1.6 shows a diagram of a potential reflectarray antenna design.

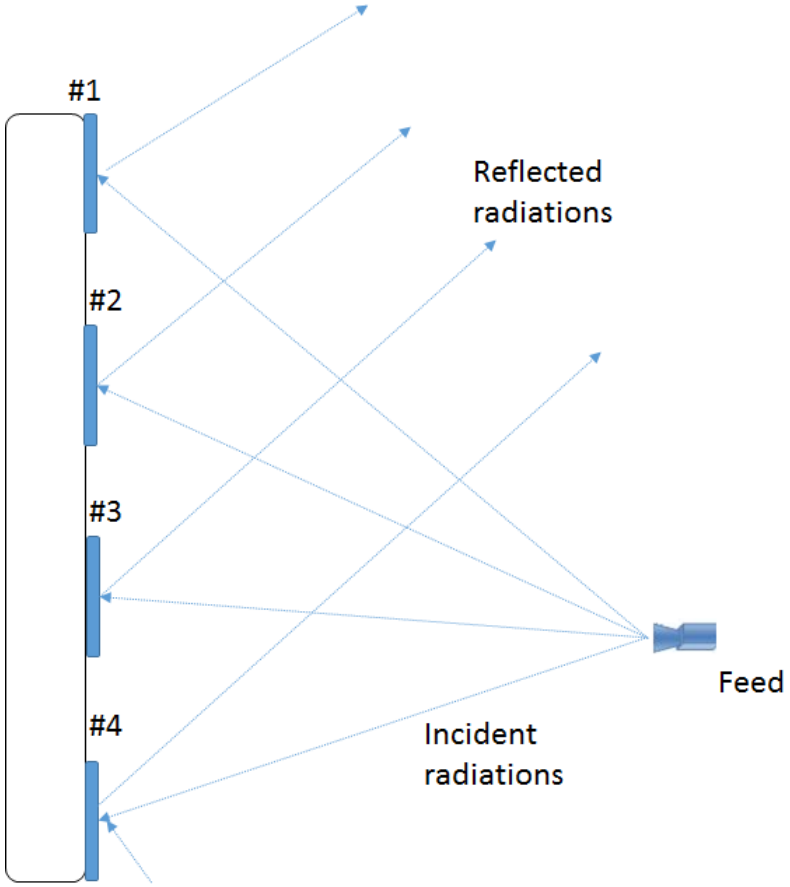

Figure 1.6: Reflectarray Antenna

1.2.2.5 Parasitic Array Antennas

Harrington [2] proposed the idea of parasitic arrays for the low cost and compact size smart antenna design. Later, Ohira [16] worked on mathematical modeling and the direction of arrival estimation for parasitic array antennas. A Yagi Uda antenna is a simple example of parasitic array antennas. Parasitic elements are driven by a single active element [17]. Passive elements, which are shorter in length, have inductive reactance and act as directors. Passive elements, which are longer in length, have capacitive reactance and act as reflectors. Fig. 1.7 shows a typical Yagi Uda antenna.

Electronically steerable parasitic array radiator (ESPAR) antennas are an area of active research due to their potential application in the next-generation wireless networks. A typical ESPAR antenna has a circular array of parasitic elements around the central feed element. Since the parasitic array approach is based on exploiting benefits of mutual inductance, antenna elements can be placed closer to each other. For beam-steering in ESPAR antennas, each passive element is loaded with a varactor diode. By varying the voltage across a varactor, the reactance of the passive antenna element is varied and the beam is steered. Fig. 1.8 shows a seven element ESPAR antenna [16].

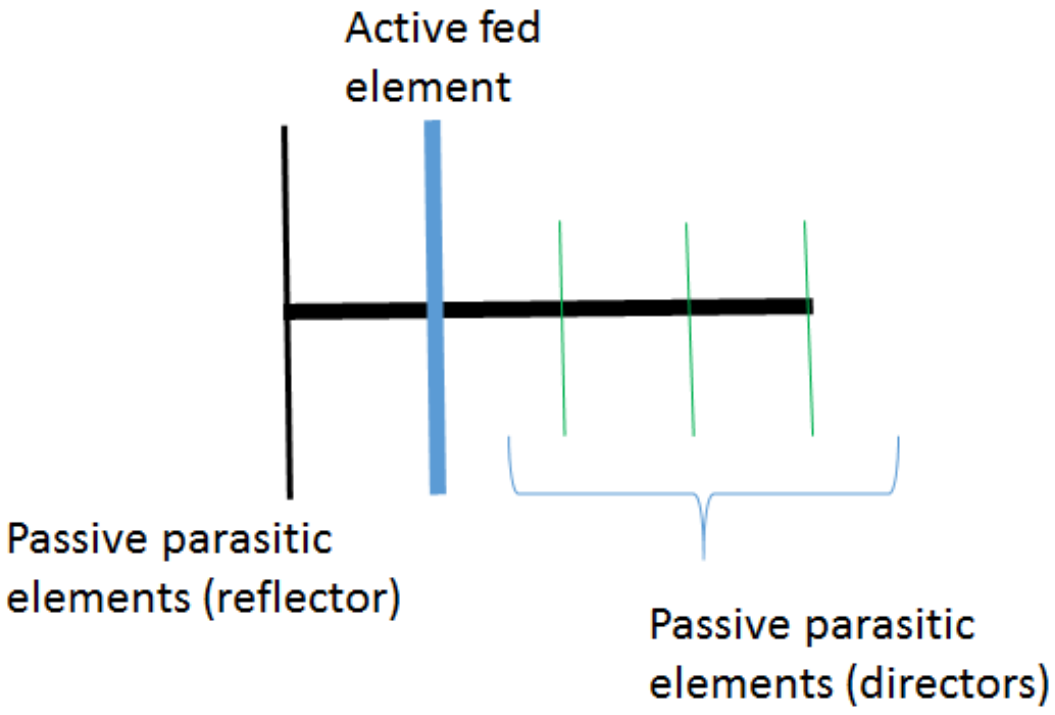

Figure 1.7: Yagi Uda Antenna

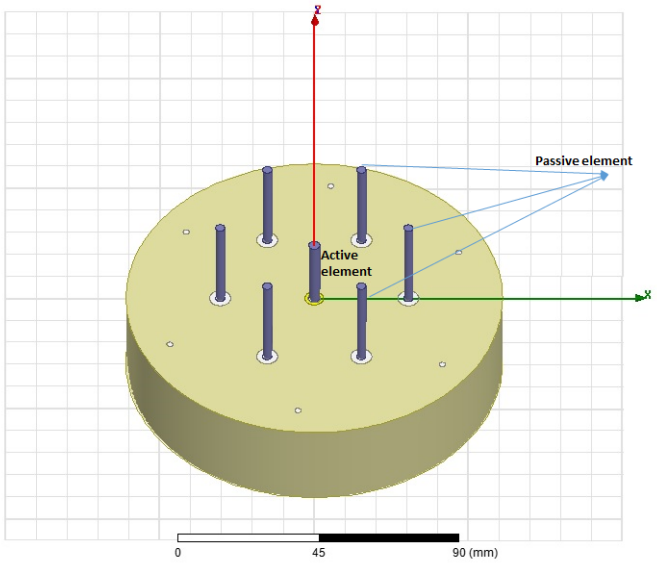

Figure 1.8: 7 Element ESPAR Antenna

1.3 Research Motivation

The aim of our research is to design a smart adaptive beamforming antenna with the following attributes:

- The smart antenna shall be low cost.
- The smart antenna design shall be simple to implement.
- The smart antenna shall be compact.
- The antenna shall have sufficient gain for the potential application in mobile stations/terminals.
- The antenna shall be relatively broadband in order to support high data rates.

To achieve the above-mentioned goals, we have proposed a novel hybrid beamforming technique. The US patent for our proposed technique was recently approved. The

proposed method uses a hybrid of phased array and parasitic array approach. It retains the advantages of both approaches. A block diagram of the proposed technique is in Fig. 1.9.

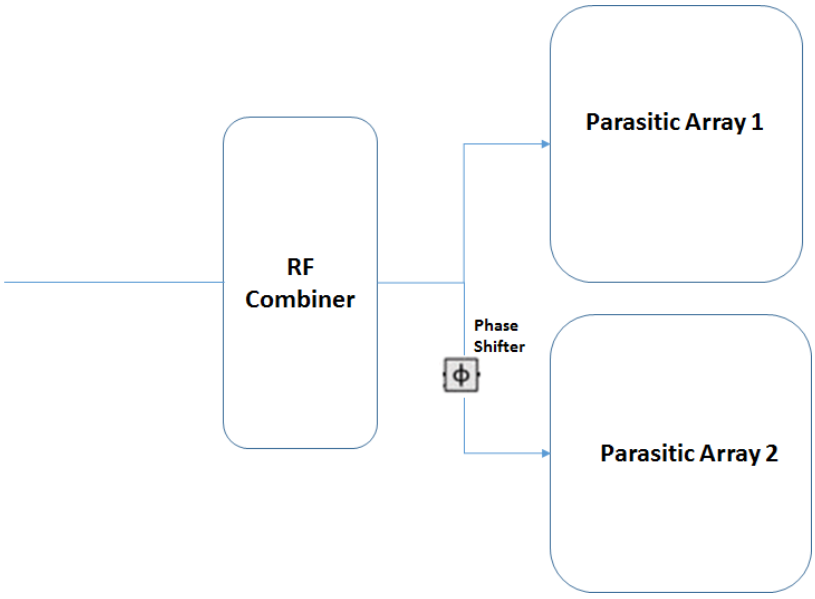

Figure 1.9: Block Diagram of Proposed Technique

1.4 Prior Art

As discussed in the previous section, an antenna beam can be steered by electronic beam steering or mechanical beam steering. In electronic beam steering, the antenna radiation pattern is steered by using switch array antennas and adaptive array antennas. Most of the smart antennas in the market are based on a switched array or a phased array approach. Switched array antennas can form beams only in discrete pre-defined directions. Therefore continuous beam-steering is not achieved in switched array antennas. Fig. 1.10 shows a circular switched array antenna. In [18] a circular switched array antenna is proposed for beam-steering in the azimuth plane. The disadvantages of the switched array antenna are:

- The desired beam is formed only at predefined angles.
- The speed of the beam-switch circuitry poses a limitation on overall beam switching rate.
- The cost of a switch array antenna is high due to redundant antennas.

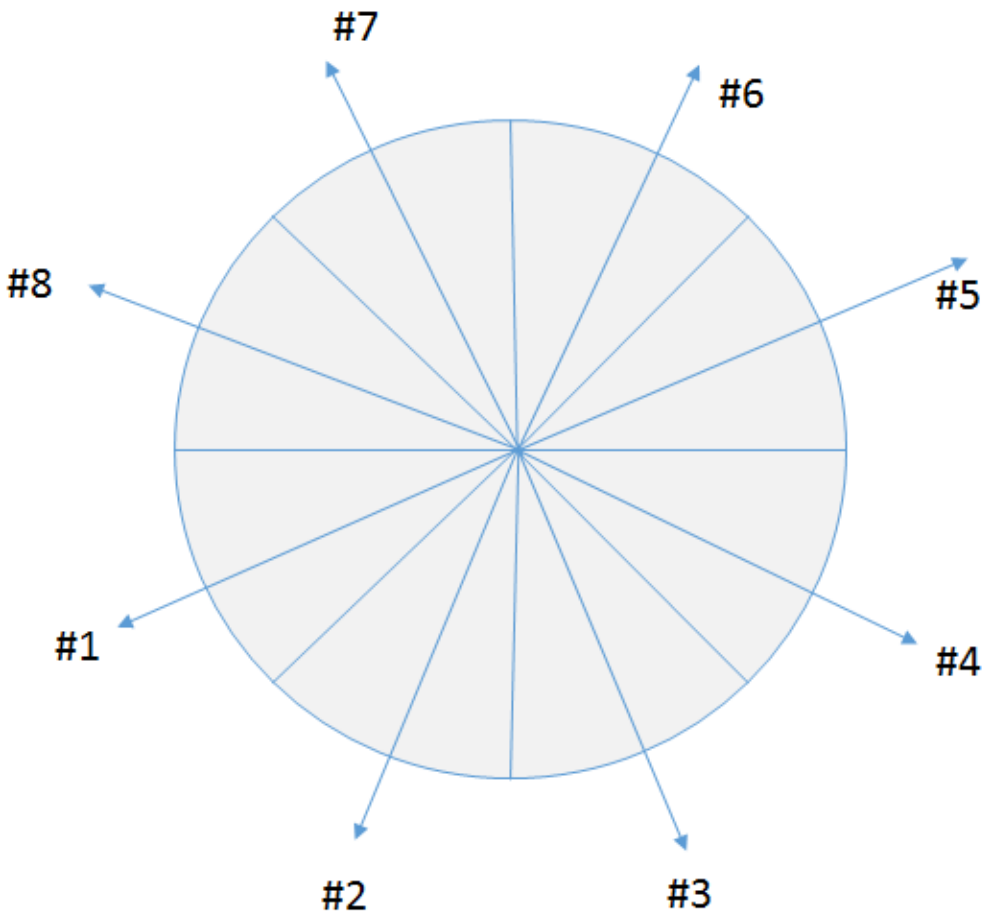

Figure 1.10: Switched Array Antenna

On the other hand, phased array antennas are capable of continuous beam-steering, but such antennas have a complex architecture and a high cost of implementation. This makes their use impractical in common communication devices such

as wireless local area networks (WLAN), mobile phones, etc. In [19], a phased array antenna is proposed for high gain applications. Phased array antennas provide a viable solution for satellite communication in commercial aviation, but due to high design cost and complexity, the application of the phased array antennas is limited. Further, each antenna element has to be separated by .7 x λ from other elements in order to avoid mutual coupling. As a result, phased array antennas are not compact in size. Moreover, phased array antennas involve phase shifters which increases the manufacturing cost of such antennas. In summary, the disadvantages of phased array antennas are:

- The high cost of implementation due to the application of phase shifters.
- A large antenna footprint.
- A lack of power efficiency.
- An overall complex structure.

If two antenna elements are placed closer than .7 x λ, the phenomena of mutual coupling will occur. ESPAR antennas exploit this phenomenon for beam-steering. The typical ESPAR antenna design consists of a circular array of parasitic monopole elements around a central active element. Optimal results are achieved when parasitic antenna elements are placed at a distance of 0.25 x λ from the active element. Parasitic monopoles are placed on the ground plane and do not require feed. Therefore, ESPAR antennas have minimal feed loss and require a single RF chain. Due to their low cost and compact size, ESPAR antennas may have a vast set of applications in next-generation wireless communication devices.

In ESPAR antennas each parasitic element is loaded with a varactor. By varying the reactance of the varactor, the phase of the induced current can be varied. Fig. 1.11 shows an ESPAR antenna with varactors. ESPAR antennas provide continuous 360^{o}beam-steering over azimuth plane. The typical gain of a six parasitic element ESPAR antenna is close to 7 dBi. Presence of the varactor diodes adds complexity to ESPAR antenna design. Switched parasitic array antennas are a class of ESPAR antennas in which pin diodes are used instead of varactors. This reduces the complexity of the design. However, in switched parasitic array antennas the beam is steered only at predefined angles.

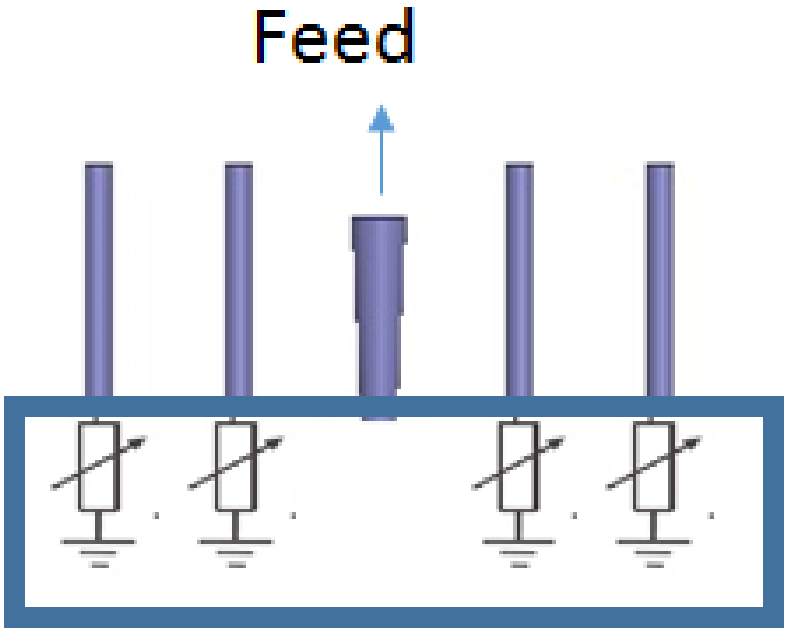

Figure 1.11: ESPAR Antenna with Varactor Diodes

We have proposed a novel hybrid beamforming smart antenna design based on our recently approved patent. A hybrid combination of a phased array and a parasitic

array is used for steering the beams. By varying the phase difference of the excitation currents in the active element and opening / shorting a sequence of the passive elements, the antenna beam is steered. Addition of phase shifters provides further degrees of freedom to achieve continuous beam-steering. The designed antenna has a single RF chain, it is low cost and it has a less complex design in comparison to phased array antennas [20]. Moreover, the antenna is capable of continuous beam-steering, which is not common amongst switched parasitic array radiator antennas. By using an innovative hybrid beamforming approach, we have overcome shortcomings of both phased array and switched parasitic array antennas. The proposed approach has the following advantages over conventional beam-steering techniques:

- The phase shifter is used only at the active elements. As a result, the designed antenna has low cost and minimal feed loss unlike phased array antennas, where each element is excited by a separate phase shifter.

- The maximum gain of the simulated antenna model is 11 dBi, which is more than a conventional 14 element ESPAR antenna.

- Continuous beam-steering is achieved by using pin diodes.

From above, it is evident that our proposed hybrid beamforming technique has advantages over ESPAR, switched parasitic array and phased array antennas. Conceptual overview of the designed antenna is shown in Fig. 1.12. In our design, the center element (active element) is made conical. Hence, the designed antenna model has a relatively large bandwidth in comparison to conventional ESPAR antennas.

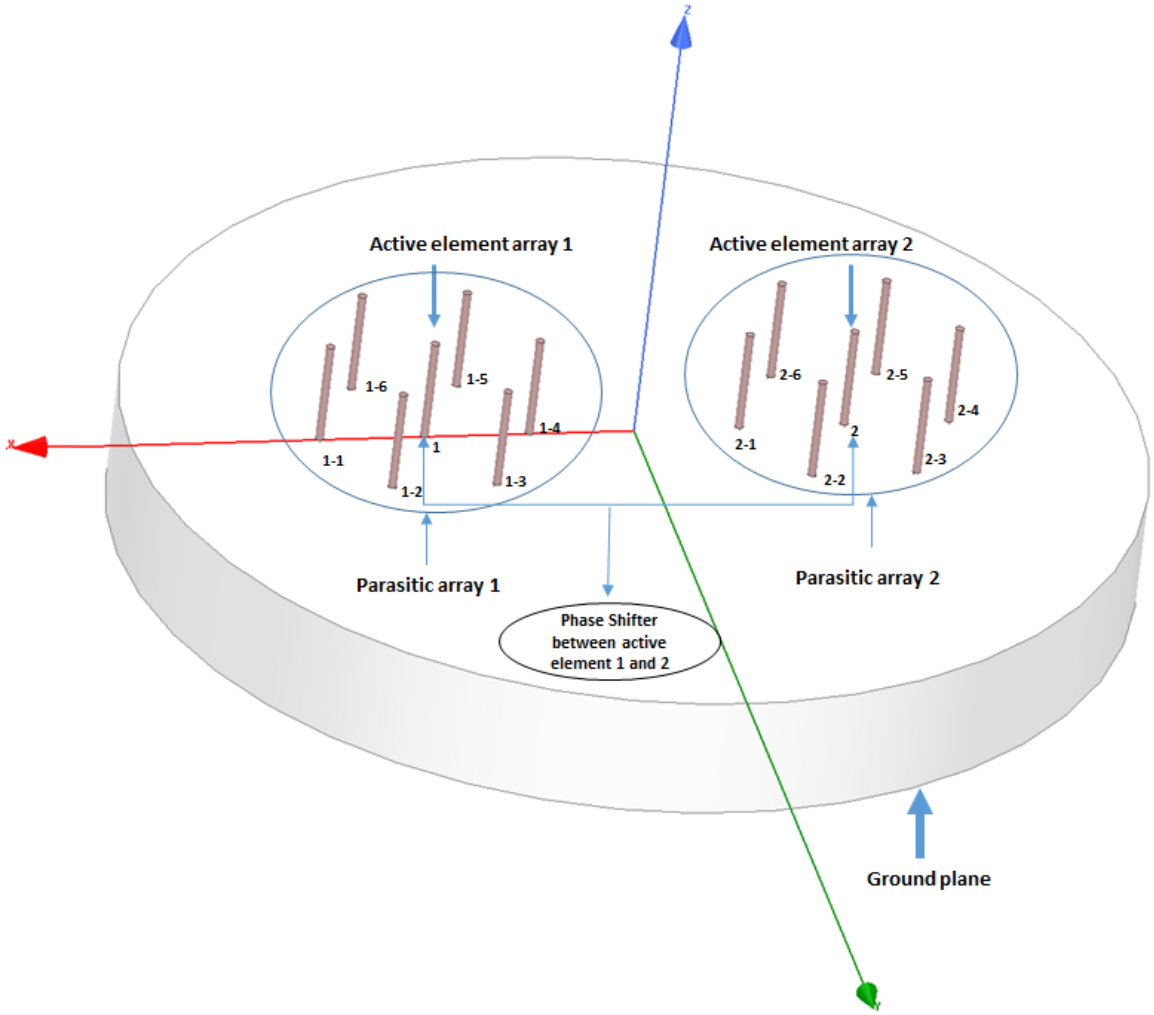

Figure 1.12: Proposed Hybrid Beamforming Antenna Design

1.5 Organization of dissertation

An antenna is basically a transducer which converts radio frequency to alternating current and vice versa. Thus far, we have covered types of antenna arrays, prior art and the motivation of our research. Next, we will cover the mathematical model behind the proposed beam-steering technique, present the simulation results, outline the antenna hardware design, motivate the application of the antenna in satellite and

commercial aviation setups, develop an antenna design for mm-Wave applications and conclude our work. Organization of the dissertation and its flow is as follows:

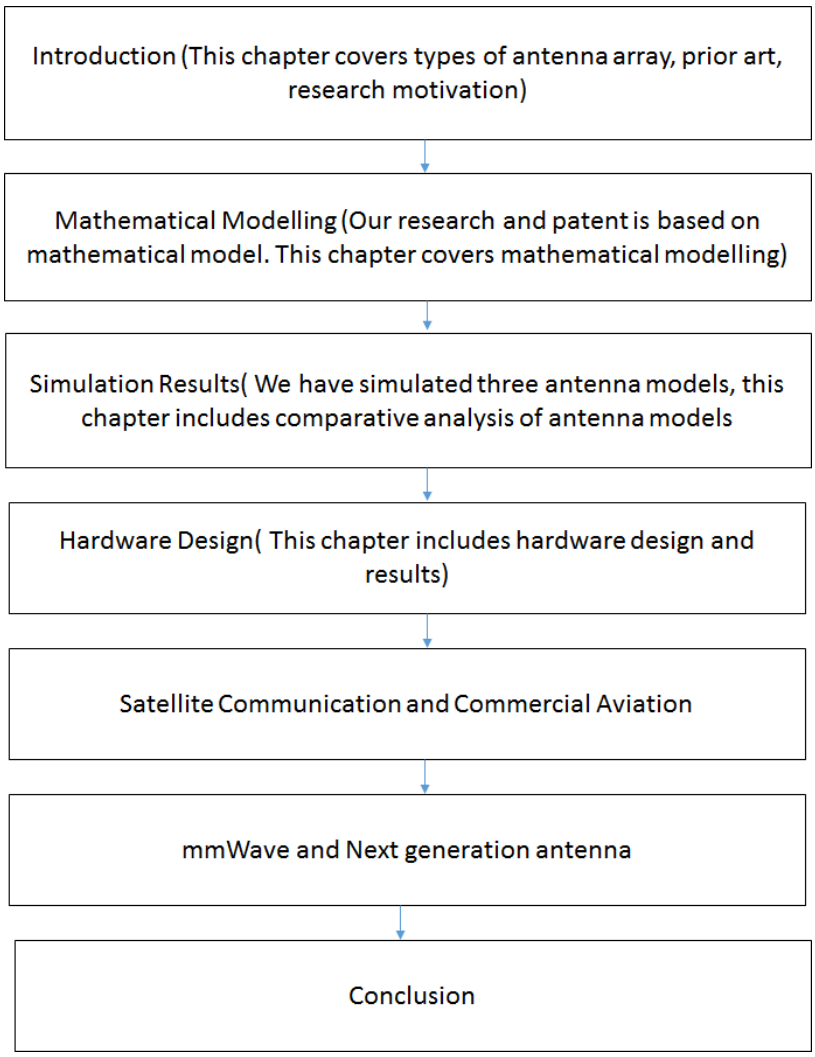

Figure 1.13: Research Methodology

CHAPTER 2

BASIC DEFINITIONS AND TERMS

2.1 Antenna

An antenna is a transducer that converts radio frequency (RF) into alternating current (AC) and vice versa. Antennas are used for the transmission and the reception of radio frequency signals. Basic level antennas are metallic conductors with a connection to the transceiver.

2.2 Smart Antennas

Smart antennas have dynamic beamforming capabilities. In these antennas the radiation pattern is formed in accordance with the environment. The design of smart antennas also requires the application of signal processing techniques.

2.3 Bandwidth

Antenna bandwidth is the range of frequencies over which the antenna performance is acceptable. The bandwidth percentage of an antenna is calculated as:

$$B.W\% = \frac{F_2 - F_1}{F_c} \tag{2.1}$$

Here, F_2 is the upper bound of the frequency of operation, F_1 is the lower bound of the frequency of operation and F_c is the carrier frequency.

2.4 Reflection Coefficient

The reflection coefficient is the ratio of the reflected electric field strength (E^-) to the incident electric field strength (E^+). For the reflection coefficient, we will be using S_{11} throughout this document. S_{11} is given as:

$$S_{11} = \frac{E^-}{E^+} \tag{2.2}$$

The reflection coefficient of a load depends on load impedance Z_L and source impedance Z_S. Fig. 2.1 shows Z_L and Z_S . Here, $S_{11}$is given as:

$$S_{11} = \frac{Z_L - Z_s}{Z_L + Z_s} \tag{2.3}$$

2.5 Voltage Standing Wave Ratio (VSWR)

VSWR is the ratio of the maximum radio frequency voltage to the minimum radio frequency voltage along the line. VSWR depends on the reflection coefficient.

$$VSWR = \frac{1 - |S_{11}|}{1 + |S_{11}|} \tag{2.4}$$

2.6 Radiation Pattern

An antenna radiation pattern is basically the variation of the antenna radiated power as a function of direction. Fig. 2.2 shows a radiation pattern in 3D.

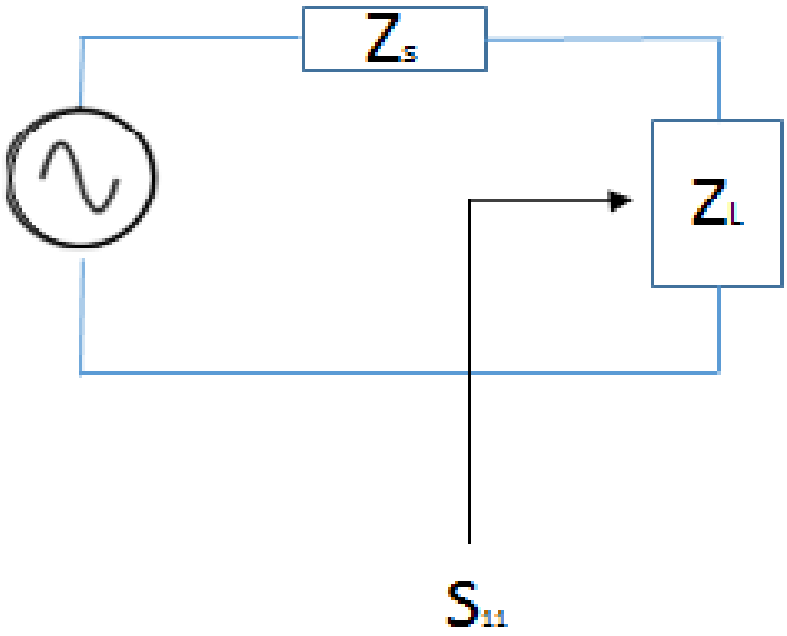

Figure 2.1: S_{11}**for given** Z_L**and** Z_S

2.7 Gain

Antenna gain is the ratio of the transmitted power in a particular direction to the power transmitted by an isotropic antenna. Gain is the product of antenna directivity and antenna efficiency. The formula for the antenna gain is given as:

$$G = D \times e \tag{2.5}$$

2.8 Antenna Efficiency

Antenna efficiency is the measure of how much antenna input power is actually radiated.

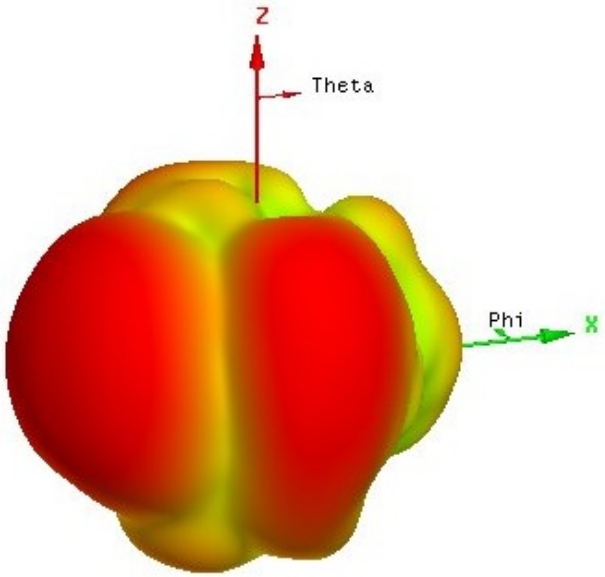

Figure 2.2: Radiation Pattern

2.9 Directivity

We can define the directivity of an antenna as the ratio of the max power to the average power per unit solid angle.

2.10 Effectively Radiated Isotropic Power

EIPR is the product of transmit antenna power and transmit antenna gain. EIRP is calculated as:

$$EIRP = P_t \times G_t \tag{2.6}$$

2.11 Azimuth Angle

The azimuth angle is the angle from the x-axis in the XY plane. Its range is from 0 - 360 degree.

2.12 Elevation Angle

Elevation Angle is the angle from z-axis in the XZ plane. Its range is from 0 - 180 degree.

2.13 Friss Transmission Equation

Friss transmission equation shows the relationship between the transmit and the receive antenna gains, transmit power, receive power, distance and frequency. The formula for the Friss transmission equation is given as:

$$\frac{P_r}{P_t} = D_r D_t \left(\frac{\lambda}{4\pi R}\right)^2 \tag{2.7}$$

2.14 Antenna Main Beam

Antenna main beam is the region around the maxima of the radiation pattern. Any point within 3 dB of the maxima is considered as part of the main lobe. This is also known as 3 dB beamwidth.

2.15 Antenna 10 dB Beamwidth

Antenna main beam is the region around maxima of the radiation pattern. Any point within 10 dB of the maxima is considered as part of the main lobe.

CHAPTER 3

MATHEMATICAL MODEL

In this chapter, we will be deriving a mathematical model for the proposed hybrid beamforming technique. First, we will be showing electromagnetic computations for the hertzian dipole, which is followed by electromagnetic calculations for the switched parasitic array antenna. Towards the end of this chapter, an electromagnetic model for the proposed beamforming technique is formulated. In the proposed model antenna radiation pattern is steered by:

- Varying the phase of the excitation current to the active elements.

- Changing the reactance of the parasitic elements.

3.1 Electric Field of Single Dipole Antenna

For calculating the electric field of a dipole antenna, an assumption is made that the antenna of length L is divided into infinite small hertzian dipoles [21] and that the current is constant over the differential length ΔL, as shown in Fig. 3.1 and Fig. 3.2 [22].

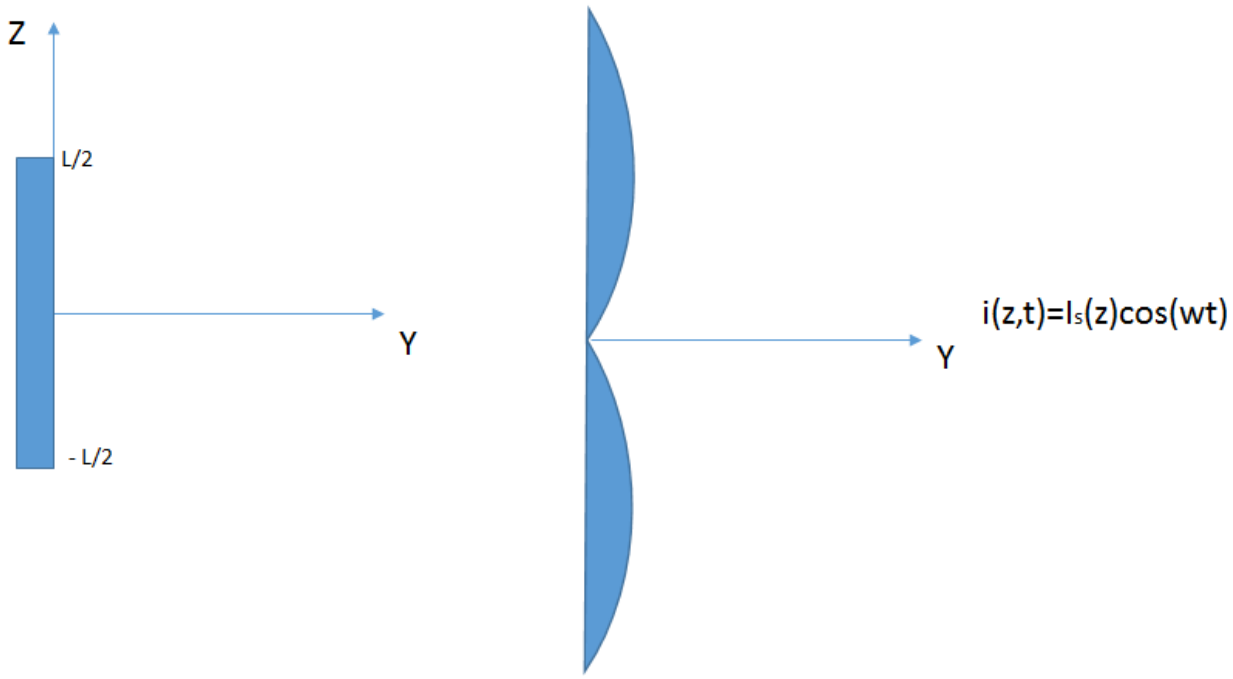

Figure 3.1: Antenna of length L

For $0 \leq Z \leq L/2$, I_s is given as [22]:

$$I_s(z) = I_0 e^{-j\alpha} \sin\left(\beta\left(\frac{L}{2} - Z\right)\right) \tag{3.1}$$

For $-L/2 \leq Z \leq 0$, I_s is given as [22]:

$$I_s(z) = I_0 e^{-j\alpha} \sin\left(\beta\left(\frac{L}{2} + Z\right)\right) \tag{3.2}$$

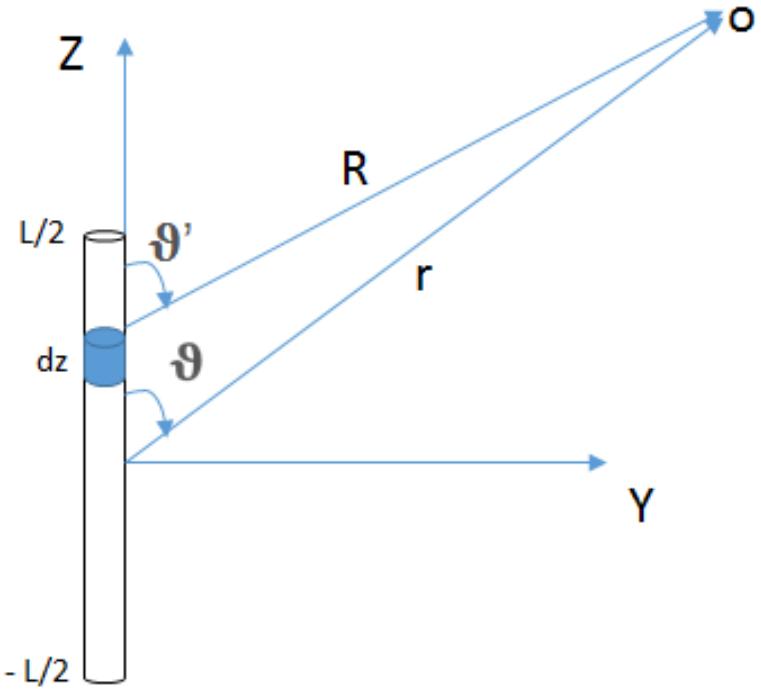

Figure 3.2: Hertzian dipole of length ΔL

The magnetic field strength of a single hertzian dipole [22] is given as:

$$\boldsymbol{H} = j\frac{I_s\beta}{4\pi}\frac{e^{-j\beta R}}{R}\sin\theta\boldsymbol{a_\phi} \tag{3.3}$$

After putting the value of I_s and integrating over the entire length of the antenna we have:

$$\boldsymbol{H} = j\frac{I_0\beta}{4\pi}\boldsymbol{a_\phi}\left[\int_{-\frac{L}{2}}^{0}\frac{e^{-j\beta R}}{R}\sin\left(\beta\left(\frac{L}{2}+Z\right)\right)\sin\theta' dz + \int_{0}^{\frac{L}{2}}\frac{e^{-j\beta R}}{R}\sin\left(\beta\left(\frac{L}{2}-Z\right)\right)\sin\theta' dz\right] \tag{3.4}$$

For far-field calculations, we have $\theta = \theta'$ and **R**=**r** (except for the terms involving

the phase) [22] as shown in Fig. 3.3, the phase portion of the overall equation can be written as:

$$e^{-j\beta R} = e^{-j\beta(r - z\cos\theta)} = e^{-j\beta r} e^{+j\beta z\cos\theta} \tag{3.5}$$

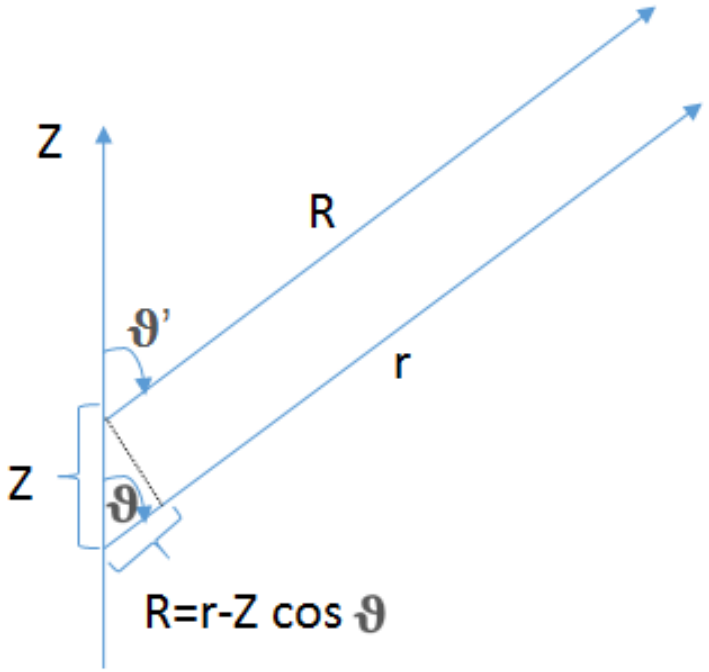

Figure 3.3: Phase Part

Here, $\beta = \frac{2\pi}{\lambda}$. After plugging in the value of $e^{-j\beta R}$ in equation (3.5) we have:

$$\boldsymbol{H} = j\frac{I_0\beta}{4\pi}\frac{e^{-j\beta r}}{r}\sin\theta\boldsymbol{a_\phi}\left[\int_{-\frac{L}{2}}^{0} e^{jz\cos\theta}\sin\left(\beta\left(\frac{L}{2}+Z\right)\right)dz + \int_{0}^{\frac{L}{2}} e^{jz\cos\theta}\sin\left(\beta\left(\frac{L}{2}-Z\right)\right)dz\right] \tag{3.6}$$

After using the integral table and further calculations [22], $\boldsymbol{H}$ can be written as:

$$\boldsymbol{H} = -j\frac{I_0 e^{-j\beta r}}{2\pi r}\left[\frac{\cos\left(\frac{\beta L}{2}\cos\theta - \cos\left(\frac{\beta L}{2}\right)\right)}{\sin\theta}\right]\boldsymbol{a}_\phi \tag{3.7}$$

$$\boldsymbol{E} = -Z_0\boldsymbol{a_r} \times \boldsymbol{H} \tag{3.8}$$

$$\boldsymbol{E} = jZ_o\frac{I_0 e^{-j\beta r}}{2\pi r}\left[\frac{\cos\left(\frac{\beta L}{2}\cos\theta - \cos\left(\frac{\beta L}{2}\right)\right)}{\sin\theta}\right]\boldsymbol{a}_\theta \tag{3.9}$$

3.2 Electric Field of a Half Wave Dipole Antenna Array

For the calculating electric field of the antenna array, we assume that two hertzian dipoles are placed alongside each other as shown in Fig. 3.4.

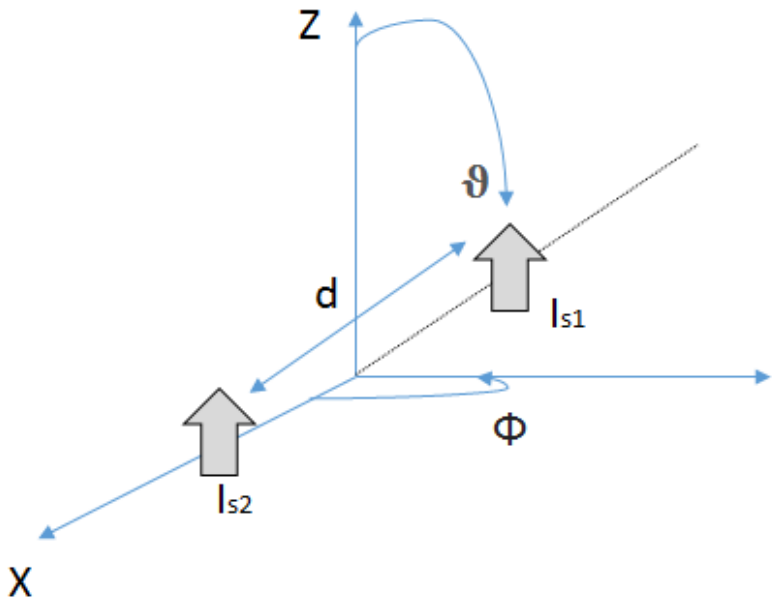

Figure 3.4: Half Wave Dipole

The electric field of a hertzian dipole is given as:

$$\boldsymbol{E} = jZ_0 \frac{I_s \beta}{4\pi} \frac{e^{-j\beta r}}{r} \sin\theta \boldsymbol{a_\theta} \tag{3.10}$$

Assuming $\theta = \frac{\pi}{2}$, E_1 and E_2 are [21] are given by:

$$\boldsymbol{E_1} = jZ_0 \frac{I_{s1} \beta}{4\pi} \frac{e^{-j\beta r_1}}{r_1} \boldsymbol{a_\theta} \tag{3.11}$$

$$\boldsymbol{E}_2 = jZ_0 \frac{I_{s2} \beta}{4\pi} \frac{e^{-j\beta r_2}}{r_2} \boldsymbol{a_\theta} \tag{3.12}$$

Let $|I_{s1}| = |I_{s2}| = I_0$ and α be the phase difference. Subsequently, $I_{s2} = I_0 e^{j\alpha}$. Fig. 3.5 depicts that for far-field $\theta_1 = \theta_2 = \theta$ and $r_1 = r_2 = r$ except for the phase portion $j\alpha$ [21].

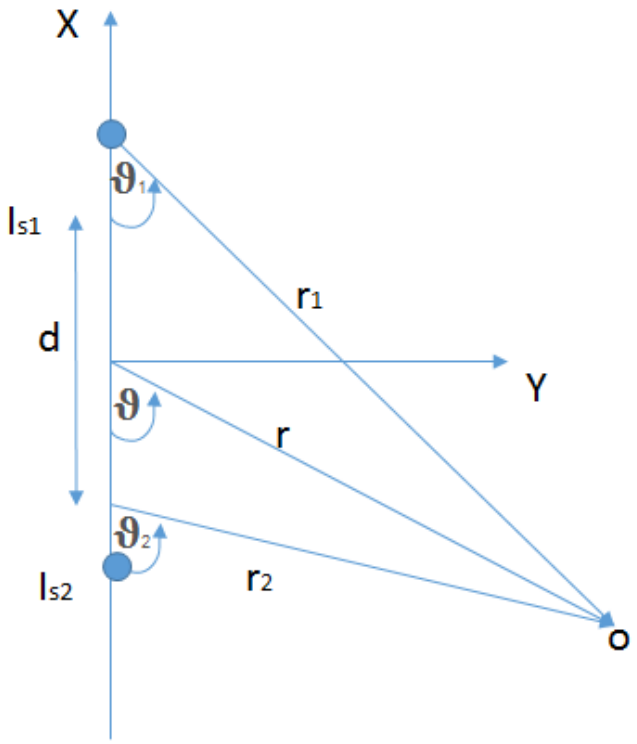

Figure 3.5: $\theta_1 = \theta_2 = \theta$ **and** $r_1 = r_2 = r$

For the phase part, we have:

$$r_1 = r + \frac{d}{2}\cos\theta \tag{3.13}$$

$$r_2 = r - \frac{d}{2}\cos\theta \tag{3.14}$$

The total Electric field is given by:

$$E_{tot} = E_1 + E_2 \tag{3.15}$$

$$E_{tot} = \frac{jZ_0 I_0 l\beta}{4\pi}\left[\frac{e^{-j\beta\left(r+\frac{d}{2}\cos\theta\right)}}{r} + \frac{e^{j\alpha}e^{-j\beta\left(r-\frac{d}{2}\cos\theta\right)}}{r}\right] \tag{3.16}$$

$$E_{tot} = \frac{jZ_0 I_0 l\beta}{4\pi}\frac{e^{-j\beta r}}{r}e^{j\frac{\alpha}{2}}\left[e^{-j\left(\frac{\beta d}{2}\cos\theta+\frac{\alpha}{2}\right)} + e^{+j\left(\frac{\beta d}{2}\cos\theta+\frac{\alpha}{2}\right)}\right] \tag{3.17}$$

$$E_{tot} = \frac{jZ_0 I_0 l\beta}{4\pi}\frac{e^{-j\beta r}}{r}2e^{j\frac{\alpha}{2}}\cos\left(\frac{\beta d}{2}\cos\theta + \frac{\alpha}{2}\right) \tag{3.18}$$

For $\beta = \frac{2\pi}{\lambda}$, E_{tot} becomes:

$$E_{tot} = \underbrace{\frac{jZ_0 l I_0}{2\lambda}\frac{e^{-j\beta r}}{r}e^{j\frac{\alpha}{2}}}_{Element\,Factor}\underbrace{2\cos\left(\frac{\beta d}{2}\cos\theta + \frac{\alpha}{2}\right)}_{Array\,Factor} \tag{3.19}$$

3.3 Mathematical Model for the Proposed Hybrid Beamforming Technique

The proposed hybrid beamforming technique is based on a mathematical model. Fig. 3.6 shows an antenna equivalent model for the mathematical derivation of the array factor of the hybrid beam-steering antenna. Two arrays of six parasitic elements and one active element are placed on the ground plane at a distance of 1.25 $\times \lambda$. A distance of 1.25 $\times \lambda$ is used in order to avoid mutual coupling between parasitic elements of both arrays. Length of monopole elements is selected as λ / 4. Ground plane transforms monopole elements with their image to dipoles of length λ / 2 (half wave dipole). From classic antenna theory [21], the electric field of an antenna array is given as:

$$E(\theta,\phi)_{tot} = E(\theta,\phi)_{elem} \times A.F(ArrayFactor) \tag{3.20}$$

In our case, we have two arrays, let γ be the phase difference between the excitation current of each array. $E(\theta,\phi)_{tot}$ is expressed as:

$$E(\theta,\phi)_{tot} = E(\theta,\phi)_{elem} \times (A.F_1 + A.F_2) \times e^{j\gamma} \tag{3.21}$$

$$E(\theta,\phi)_{elem} = \frac{jZ_0}{2\lambda}\frac{e^{-j\beta r}}{r} \tag{3.22}$$

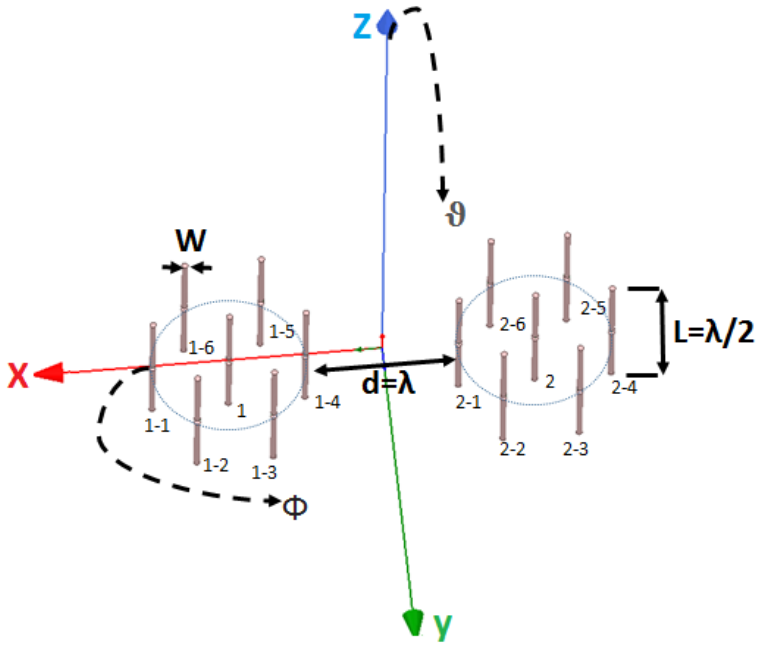

Figure 3.6: Hybrid Beamforming Antenna.

From Fig. 3.6 we can see that each array has six parasitic elements and one active element. There is a phase difference of γ between excitation currents to the active elements. Length L of the equivalent dipole model is λ / 2 and W is the width of the dipole elements. We have used W=0.02 $\times$ λ in our calculations. Vector Effective Length Equivalent Weight Vector (VEL-EWV) model is proposed in [23] for characterizing the ESPAR antenna radiation pattern. Array factor of an ESPAR antenna is the product of the port current, the vector effective length and the steering varactor [24], i.e.:

$$A.F = \sum_{m=0}^{M} l_m(\theta) i_m a_m(\theta, \phi) \tag{3.23}$$

where i_m is the port current, $l_m(\phi)$ is the vector effective length and $a_m(\theta, \phi)$ is the steering vector. Current and voltage relationship on the dipole elements is given

by [24, 20, 25]:

$$I = [\ i_o\ i_1\ i_2\ i_3\ i_4\ i_5\ i_6\ ]^T \tag{3.24}$$

$$V = [\ v_o\ v_1\ v_2\ v_3\ v_4\ v_5\ v_6\ ]^T \tag{3.25}$$

$$I = YV \tag{3.26}$$

$$I = \begin{bmatrix} y_{00} & y_{01} & y_{02} & y_{03} & y_{04} & y_{05} & y_{06} \\ y_{01} & y_{11} & y_{12} & y_{13} & y_{14} & y_{15} & y_{16} \\ y_{02} & y_{21} & y_{22} & y_{23} & y_{24} & y_{25} & y_{26} \\ y_{03} & y_{31} & y_{32} & y_{33} & y_{34} & y_{35} & y_{36} \\ y_{04} & y_{41} & y_{42} & y_{43} & y_{44} & y_{45} & y_{46} \\ y_{05} & y_{51} & y_{52} & y_{53} & y_{54} & y_{55} & y_{56} \\ y_{06} & y_{61} & y_{62} & y_{63} & y_{64} & y_{65} & y_{66} \end{bmatrix} \begin{bmatrix} v_o \\ v_1 \\ v_2 \\ v_3 \\ v_4 \\ v_5 \\ v_6 \end{bmatrix} \tag{3.27}$$

Y_{mn} is the mutual admittance between m_{th} and n_{th} element. Due to the symmetrical design of the circular array elements, the admittance matrix can be simplified as shown in equation (3.28). In our model, we are using the admittance matrix values which were calculated in [24] by using NEC.

$$I = \begin{bmatrix} y_{00} & y_{10} & y_{10} & y_{10} & y_{10} & y_{10} & y_{10} \\ y_{10} & y_{11} & y_{21} & y_{31} & y_{41} & y_{31} & y_{21} \\ y_{10} & y_{21} & y_{11} & y_{21} & y_{31} & y_{41} & y_{31} \\ y_{10} & y_{31} & y_{21} & y_{11} & y_{21} & y_{31} & y_{41} \\ y_{10} & y_{41} & y_{31} & y_{21} & y_{11} & y_{21} & y_{31} \\ y_{10} & y_{31} & y_{41} & y_{31} & y_{21} & y_{11} & y_{21} \\ y_{10} & y_{21} & y_{31} & y_{41} & y_{31} & y_{21} & y_{11} \end{bmatrix} \begin{bmatrix} v_o \\ v_1 \\ v_2 \\ v_3 \\ v_4 \\ v_5 \\ v_6 \end{bmatrix} \tag{3.28}$$

Only active elements are excited by the feed in case of ESPAR antennas. Therefore, the port voltages of the parasitic elements are only dependent on the induced current. The expression for the port voltage is given as [23, 26]:

$$V = \begin{bmatrix} 1 \\ 0 \\ 0 \\ 0 \\ 0 \\ 0 \\ 0 \end{bmatrix} v_s - XI = v_s U_1 - XI \tag{3.29}$$

By putting the value of V in equation (3.8) we can reach to the final expression of the port current i_m:

$$I = Y(v_s U - XI) \tag{3.30}$$

$$I = Y v_s U - YXI \tag{3.31}$$

$$I + YXI = Yv_sU \tag{3.32}$$

$$I(Y^{-1} + X) = v_sU \tag{3.33}$$

$$I = (Y^{-1} + X)^{-1}v_sU \tag{3.34}$$

$$I = (Z_{mn} + X)^{-1}V_s \tag{3.35}$$

$$X = diag\left[z_0, jx_1, jx_2, jx_3, jx_4, jx_5, jx_6\right] \tag{3.36}$$

$$V_s = \left[v_s\ 0\ 0\ 0\ 0\ 0\ 0\right]^T \tag{3.37}$$

Vector effective length used in equation (3.23) for far-field calculation is given by:

$$l_m = l_m^0\left(1 - \alpha_m x_m\right)\sin\theta \tag{3.38}$$

Here, l_m^0 and α_m are the structural parameters of the ESPAR antenna design and their values are calculated by using NEC-Win Pro [26, 23, 27] , X_m is the reactance set of parasitic elements, m varies from 0 to 6 for a seven element ESPAR antenna. Further, l_0 is calculated as:

$$l_0 = l_0^o\left(1 - j\alpha_o Z_{in}\right)\sin\theta \tag{3.39}$$

In the proposed hybrid beamforming technique we are using two parasitic arrays,

where γ is the phase difference between the excitation currents to the active elements of both arrays. Fig. 3.7 shows the top view of arrays in the XY plane. The steering vector is calculated as:

$$\alpha_1(\theta,\phi) = \sum_{m=1}^{M} e^{jk(\sin(\theta)\cos(\phi)x_m + \sin(\theta)\sin(\phi)y_m)} \tag{3.40}$$

$$\alpha_2(\theta,\phi) = \sum_{m=1}^{M} e^{jk(\sin(\theta)\cos(\phi)x'_m + \sin(\theta)\sin(\phi)y'_m)} \tag{3.41}$$

$$A.F_1 = \sum_{m=0}^{M} l_m(\theta) i_m a_{1m}(\theta,\phi) \tag{3.42}$$

$$A.F_2 = \sum_{m=0}^{M} l_m(\theta) i_m a_{2m}(\theta,\phi) \tag{3.43}$$

$$E(\theta,\phi)_{tot} = E(\theta,\phi)_{elem} \left[\sum_{m=0}^{M} l_m(\theta) i_m a_{1m}(\theta,\phi) + \sum_{m=0}^{M} l_m(\theta) i_m a_{2m}(\theta,\phi) \right] e^{j\gamma} \tag{3.44}$$

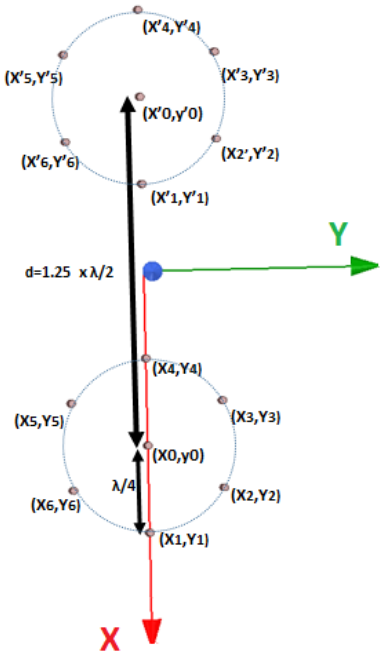

Figure 3.7: Top view in X-Y Axis.

The overall directivity is given by [26]:

$$D(\theta,\phi) = 4\pi \frac{r^2|E\theta,\phi)|^2}{Z_o|v_o|^2 Re\left(\frac{1}{Z_{in}}\right)} \tag{3.45}$$

By further simplifying equation (3.43), we can arrive at [26]:

$$D(\theta,\phi) = \frac{\pi Z_0 \sin\theta|\sum_{m=0}^{M} l_m i_m|_{Zs=0} a_m(\theta,\phi)|^2}{\lambda^2|v_s|^2 Re\left(\frac{1}{Z_{in}}\right)} \tag{3.46}$$

The antenna is simulated in Ansoft High Frequency Structure Simulator (HFSS) after the mathematical modeling. Antenna design parameters are given in Table 6.1.

Table 3.1: Parameters for Mathematical Model

Frequency	2.45 GHz
Monopole Radius	$0.01 \times \lambda$=1.2244 mm
Ground Radius	$1.2 \times \lambda$=146.93 mm
Monopole Length	$\lambda/4$=30.61 mm
Ground Skirt Hight	$\lambda/4$=30.61 mm
Distance Between Arrays	$1.25 \times \lambda$= 153.05 mm

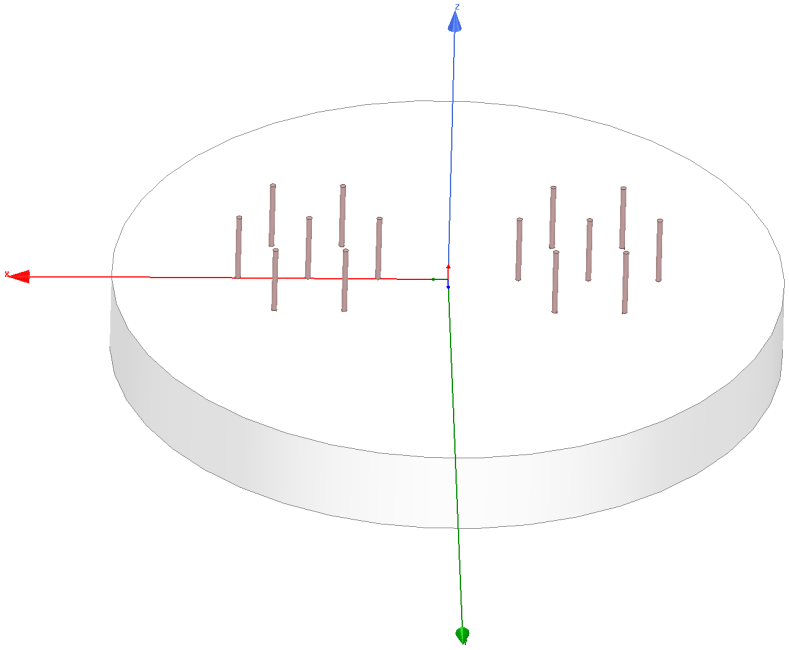

Figure 3.8: Simulated Hybrid Antenna.

We have compared the simulation results with the mathematical results to ensure the accuracy of overall design. The simulated antenna model is shown in Fig. 3.8. Both results are in close agreement with each other. Ansoft HFSS uses the Finite Element Method (FEM) for computations. Fig. 3.9 shows a comparison of the FEM and the mathematical model for a maxima at 270°.

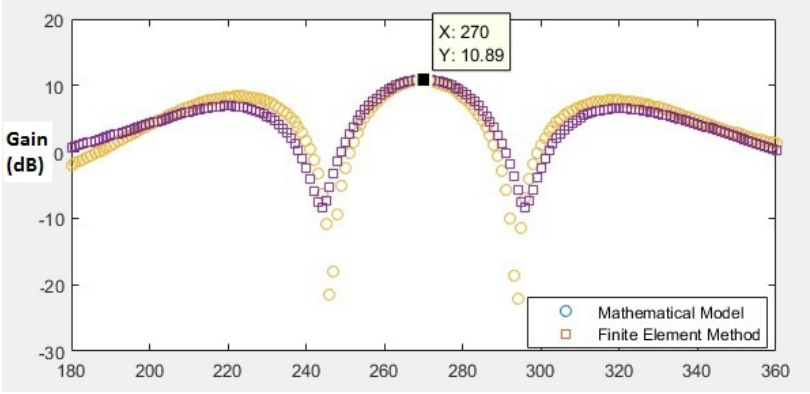

Figure 3.9: FEM and Mathematical Model Comparison.

Once we add a phase shift of 50° between the currents of the active elements, the maxima is shifted towards the left by 5° and a beam is formed at 265°, this is shown in Fig. 3.10.

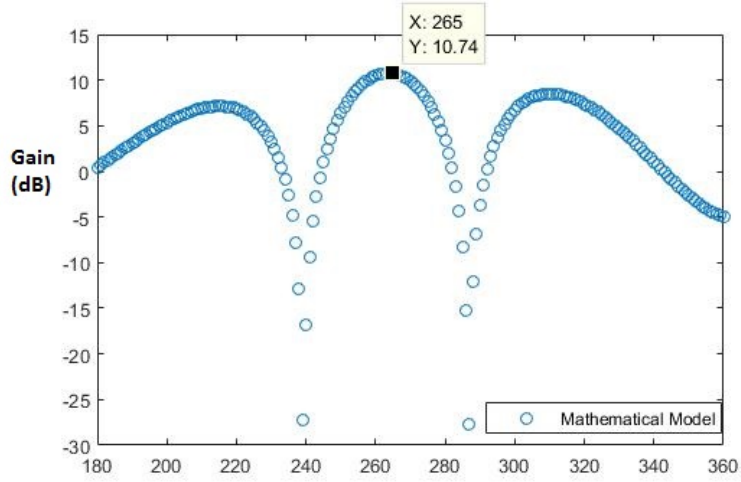

Figure 3.10: Mathematical Model for Maxima at 265^0.

When the phase difference of 70° is added, the maxima is formed at 260° as shown in Fig. 3.11.

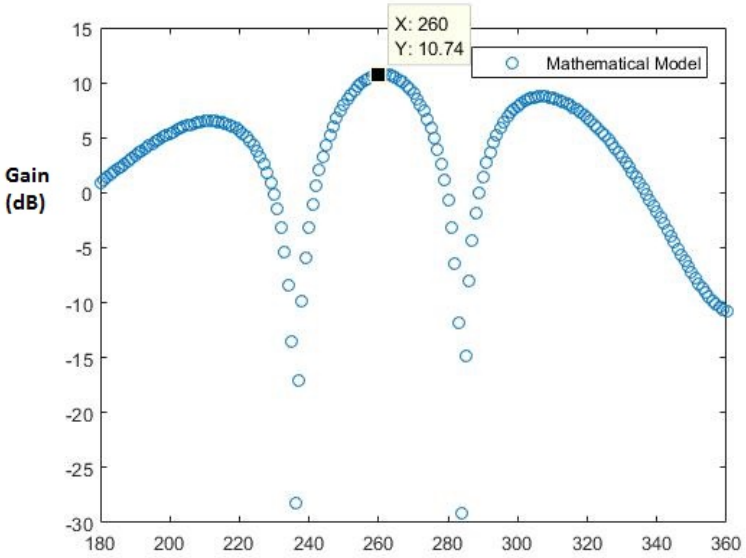

Figure 3.11: Mathematical Model for Maxima at 260^0.

From above, one can see that the mathematical model and finite element methods are in line with each other.

CHAPTER 4

SMART ANTENNA DESIGN FOR 2.5 GHZ

In this chapter, we have discussed the design of a smart antenna centered at 2.5 GHz. Generally, smart antennas have phased arrays or parasitic arrays. In our design, we have used both approaches in conjunction with each other in order to maximize their advantages. Antenna design consists of two circular arrays on a ground plane, separated by a distance of $1.25\times\lambda$ from each other. Each circular array has one active and six parasitic elements. There is a digital phase shifter between both active elements for varying the phase shift. The antenna is first simulated in Ansys HFSS, after optimization of the design parameters in HFSS. After antenna fabrication, the antenna radiation pattern is verified in an anechoic chamber. A peak gain of 11 dBi is achieved. The gain of our antenna is twice as that of a conventional ESPAR antenna. The active element of each array is a conical monopole, whereas the parasitic elements are cylindrical monopoles. The antenna has a relatively broader bandwidth in comparison to traditional ESPAR antenna models because the active element is conical. Antenna resonates over a broad range of frequencies. Fig. 4.1 shows a conical monopole with the flare angle θ_0. Z_{in} of an antenna with a flare angle θ_0 and length a is given as [28]:

$$Z_{in} = Z_0 \frac{1\text{-}\frac{\beta}{\alpha}}{1+\frac{\beta}{\alpha}} \tag{4.1}$$

$$Z_o = 60 \ln \left(\cot \left(\frac{\theta_0}{2} \right) \right) \tag{4.2}$$

$$\frac{\beta}{\alpha} = e^{-2ika}.F(a) \tag{4.3}$$

Here Z_0 is the characteristic impedance of an antenna and $\frac{\beta}{\alpha}$ is the ratio of the amplitudes of reflected waves and outwardly traveling TEM waves [28].

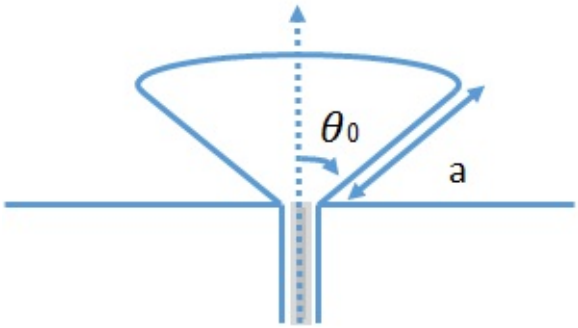

Figure 4.1: Conical Antenna with Flare θ_0.

Unlike conventional ESPAR antennas, the radiation pattern of our designed antenna is adaptive. We can get up to three beams by using a single transmit chain. The antenna is first simulated in HFSS. Subsequently, the antenna is fabricated. We have validated and compared hardware results with the simulated model. Antenna system design process consists of following:

- The design of the Aluminum ground plane
- PCB design
- Component soldering

4.1 Design Enhancement

Wireless communication systems are replacing wired communication systems. The current frequency spectrum is depleting and it has become a precious commodity. In order to further increase data rates and improve spectral efficiency, extensive use of smart antennas is imminent in next-generation communication devices. Smart antennas have the capability of adaptive beamforming. The antenna beam is steered in accordance with the environment. Antenna radiation pattern can be steered by a mechanical beam steering approach or by an electronic beam steering approach. The antenna is physically moved in case of mechanical beam steering. This approach is not desirable once we take into account antenna size and weight. Mechanical beam steering involves moving parts. Therefore, it is prone to wear and tear. Such a design results in high power consumption due to the use of mechanical motors. Conventionally, electronic beam steering is achieved by using phased array antennas. In phased array antennas, the radiation pattern is changed by changing the phase of an individual element in an antenna array. Phased array antenna design involves phase shifters. Therefore, such antennas are not cost effective. Size of phased array antennas is not compact because each antenna element has to be separated by at least half of the wavelength from other elements to avoid mutual coupling.

Currently, the cost of production and size of smart antennas pose a limitation for practical application of smart antennas in everyday communication devices. ESPAR antennas provide a cost-effective and compact solution for the smart antenna design. If two antenna elements are in close proximity, mutual coupling takes place. ESPAR antennas take advantage of the mutual coupling to change the direction of the beam radiated. Therefore, such antennas are cost-effective and require less space

in comparison to the phased array antennas. Traditional ESPAR antennas have one central active element, which is surrounded by an array of passive elements, where excitation is provided to the central element only. As parasitic elements are placed closer than $\lambda/2$ to the active element, current is induced in the parasitic elements. By varying the phase of the induced current in the parasitic elements, the antenna beam can be steered. Fig. 4.2 shows the conceptual overview of an ESPAR antenna. Here, parasitic elements are loaded with varactors. By varying reactance of the varactor, the phase of the induced current in the parasitic elements can be varied and the antenna beam is steered. In Fig. 4.3 parasitic elements are loaded with pin diodes. An open pin diode provides capacitance and a short pin diode provides a small resistance. Open elements act as directors whereas short elements act as reflectors. Yagi Uda antennas also exhibit similar behavior [29].

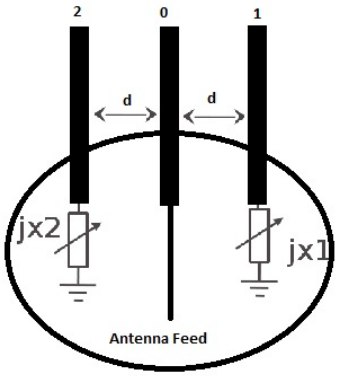

Figure 4.2: Antenna with Varactor Diodes

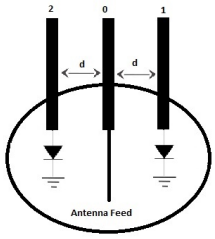

Figure 4.3: Antenna with Pin Diodes

Nowadays, parasitic antennas have gained importance because they serve as an economical and space efficient solution for next-generation communication networks. In accordance with Shannon's equation, the lesser is the interference to a system, the higher will be the throughput that it can support [30, 31], the Shannon's equation is expressed as:

$$C = B \times \log_2 \left(1 + \frac{S}{N}\right) \tag{4.4}$$

Here C is the channel Capacity, B is the channel bandwidth, (S/N) is signal to the interference noise ratio.

ESPAR antennas have the following advantages over phased array antennas:

- In ESPAR antennas, the feed network is only provided to the active element (driven element), whereas in the phased array antennas the feed network is connected to every element. Hence, ESPAR antennas have a lower feed loss as compared to the phased array antennas.

- ESPAR antennas are low cost, unlike phased array antennas. Phase shifters are not used in ESPAR antennas. As a result, the design is simple and low cost.

- Parasitic elements can be placed in close proximity of the feed element. As a result, the antenna is compact size.

We have proposed the design of a smart antenna which utilizes a hybrid of phased array and parasitic array approach for steering the radiation pattern of the antenna. Two circular parasitic arrays of monopole elements are housed over the same ground plane. Each array has one active element which is surrounded by six parasitic elements. Active / feed element is made conical for bandwidth enhancement. All other elements are cylindrical. Feed to one of the active elements has a phase shifter, which is used to regulate phase difference in antenna current of the feed elements. Fig. 4.4 provides an overview of the design topology.

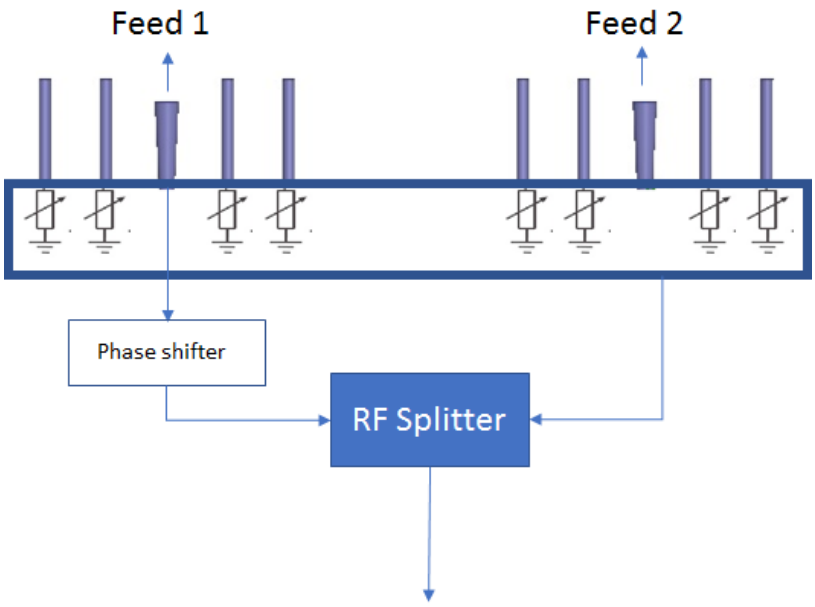

Figure 4.4: Antenna Design Overview

In our antenna design, each parasitic element is loaded with a pin diode, where opening / shorting of parasitic elements is controlled by varying voltage across the pin

diode. Unlike switched array parasitic antennas, we are achieving continuous beam steering over 360°. Beam steering is achieved by:

- Changing the phase difference in the antenna current of feed elements.

- Opening and shorting the parasitic elements.

The proposed novel hybrid beam steering approach has the following advantages over conventional beam steering techniques:

- In comparison to the phased array antenna, there is a lower loss in the feed network since the phase shifter is only connected to the active element [24].

- The designed antenna is low cost because there is only one phase shifter in our design [27].

- Simulated antenna model has a net gain of 11 dBi which is higher than ESPAR antennas. The typical gain of an ESPAR antenna is 6 dBi - 7 dBi [27].

4.2 Array of Switched Parasitic Antennas

A switched parasitic array antenna is shown in Fig. 4.5. There are two circular arrays and the feed is applied to the central element of each array.

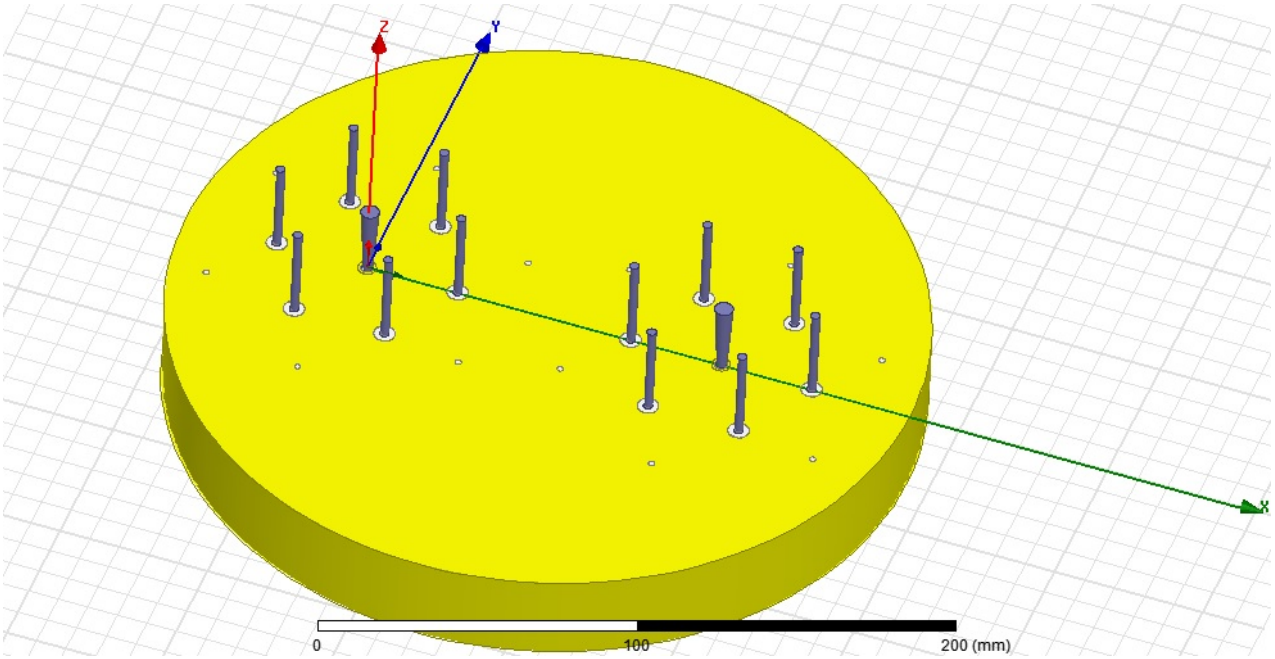

Figure 4.5: Simulated Antenna Model.

Simulated Model for 2.5 GHz Antenna

Ansys HFSS is used to simulate the proposed antenna design. We have used lumped RLC boundary for simulating the loading of parasitic elements with pin diodes in HFSS. For an open condition, RLC boundary has a capacitance of 0.35 pf and for the short condition, RLC boundary has 0.9 ohms of resistance. Parasitic elements are connected with the transmission line of $\lambda / 4$. Pin diodes are placed on the transmission line. One end of the transmission line is connected to the parasitic element and the other end is connected with the ground plane. Antenna design parameters are in Table 4.1. Top view of the antenna is shown in Fig. 4.6, whereas the side view is in Fig. 4.7.

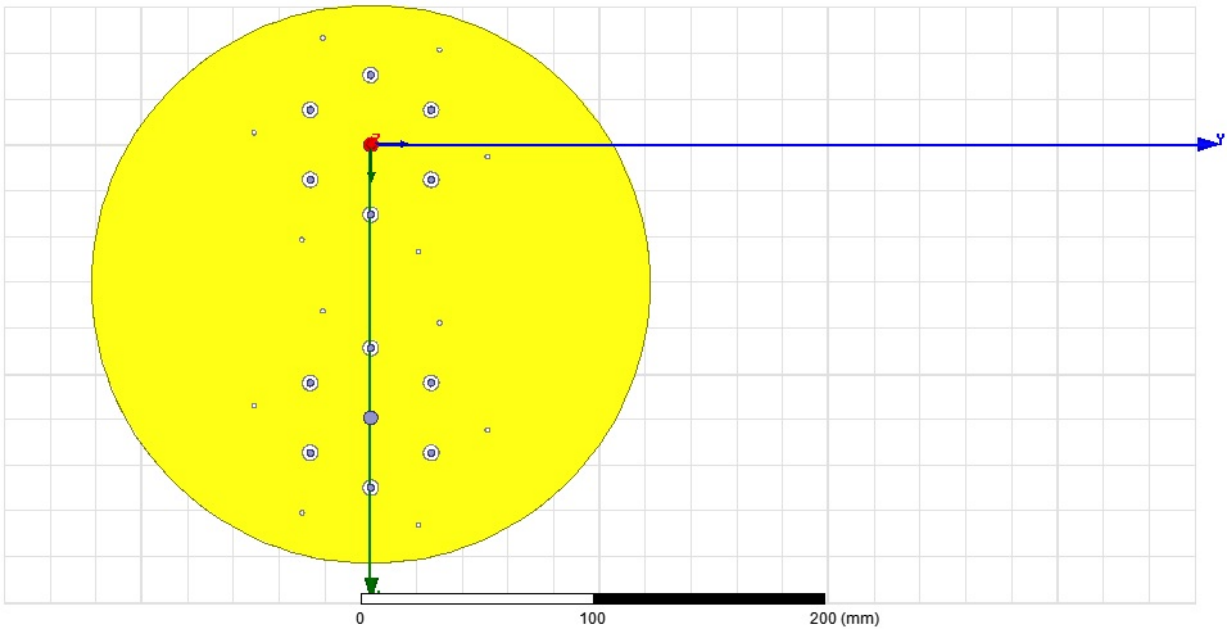

Figure 4.6: Top view of simulated antenna

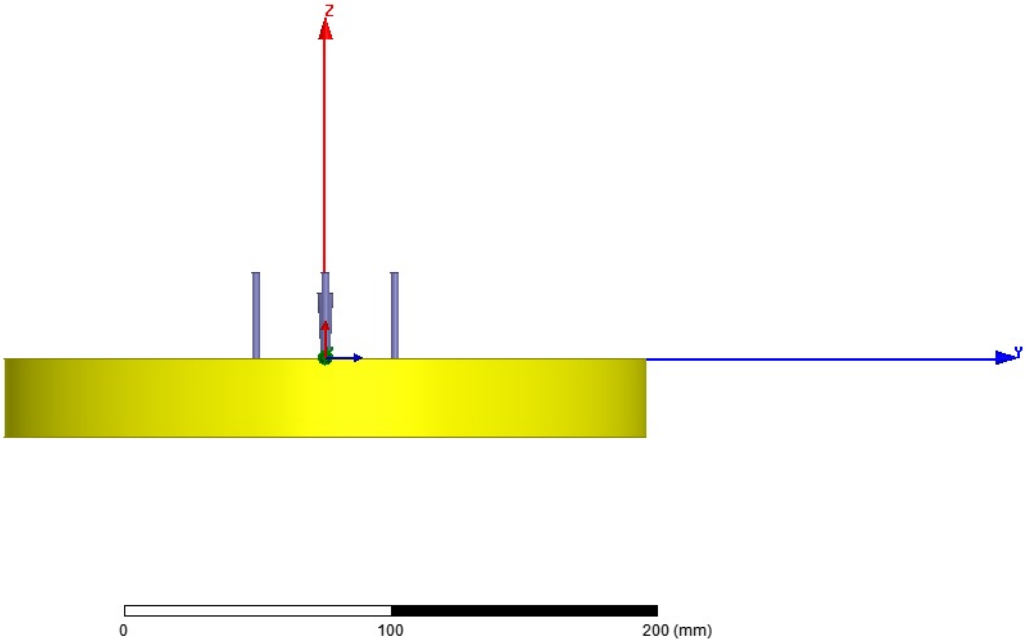

Figure 4.7: Side view of simulated antenna

Table 4.1: Antenna Design Parameters 2.5 GHz

Height of parasitic element	30 mm
Hight of conical feed	24.5 mm
Top radius of conical feed	3mm
Bottom radius of conical feed	1.8 mm
Height of ground plane	30 mm
Thickness of ground plane	4 mm
Length of transmission line	30 mm

Beam Steering Mechanics

The beam steering is achieved by using pin diodes. The beam is steered by opening and shorting of the pin diodes connected to the passive elements. Fig. 4.8 shows the designed RF PCB. Elements which are open acts as directors whereas short elements behave as reflectors [32, 33]. Yagi-Uda antennas also exhibit similar behavior [34, 35].

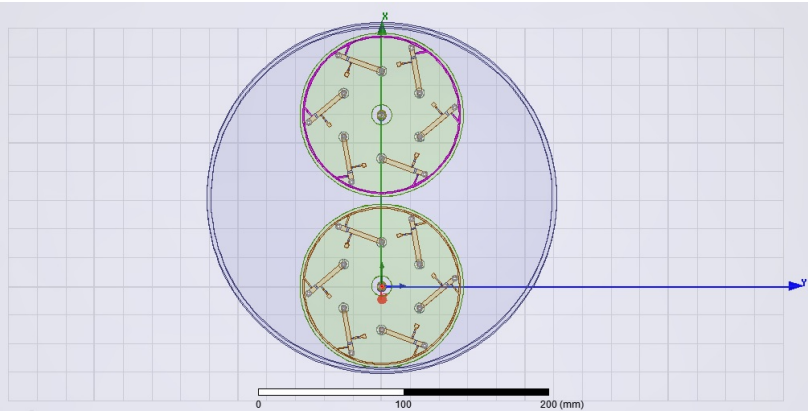

Figure 4.8: Bottom View of simulated antenna

The PCB design of the proposed antenna is shown in Fig. 4.9. 2 PCBs are mounted at the bottom of the antenna. Monopole elements are designed such that

the diameter is 1.5 mm for the portion above the ground plane and the diameter is 1 mm for the potion below the ground plane. The threaded portion of the monopole element passes through the Teflon. We will be using the term *element pin* for threaded portion of monopole element (the portion below ground). The radius of the element pin and Teflon is calculated by using appcad, such that 50 ohm impedance is achieved.

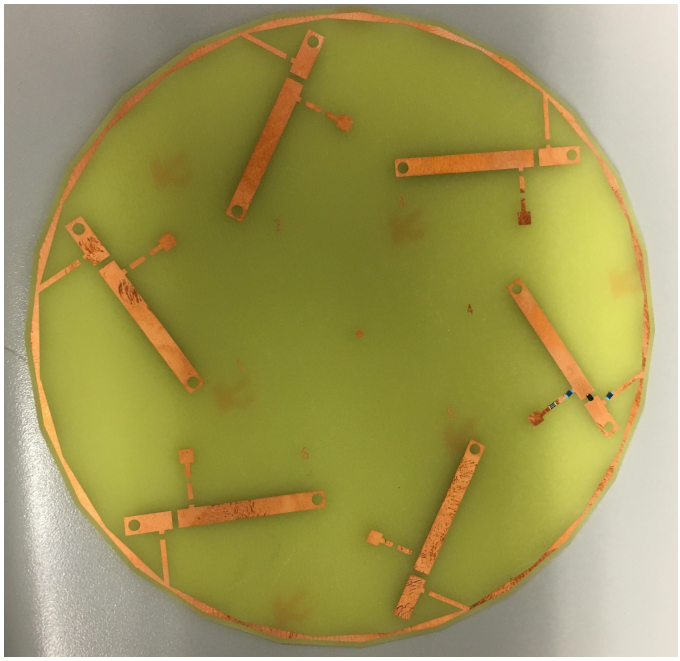

Figure 4.9: RF PCB.

Fig. 4.10 shows the biasing circuit that has a pin diode, 100 nH inductor and a 100 ohm resistor. In HFSS, we have loaded the lumped ports with a 100 ohms resistor and a 100 nH inductor.

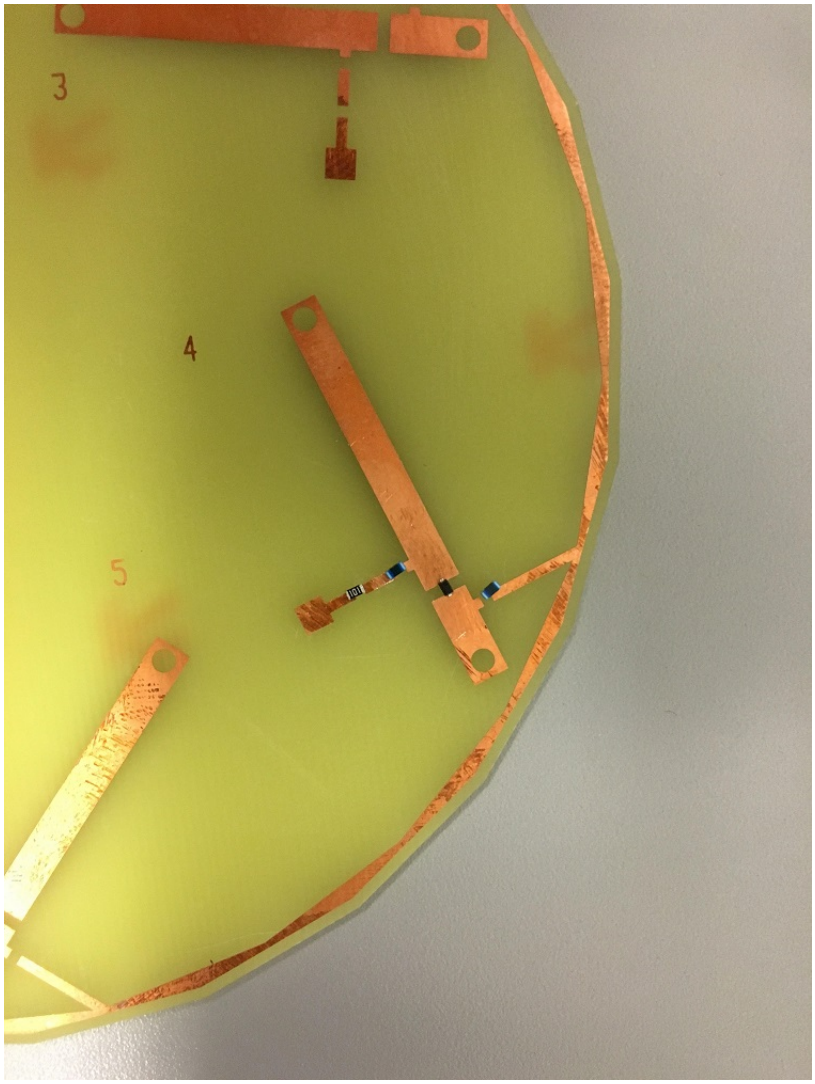

Figure 4.10: Biasing circuit with pin diode.

4.3 Antenna Hardware

The antenna is designed at 2.5 GHz. Center element is conical with 3 mm radius at the top of the cone and 1.8 mm radius at the bottom of the cone. The designed antenna is shown in Fig. 4.11. One can see there are two identical circular arrays of parasitic elements. Each array has a single active element. There is a digital phase

shifter between the active elements to support the required phase shift.

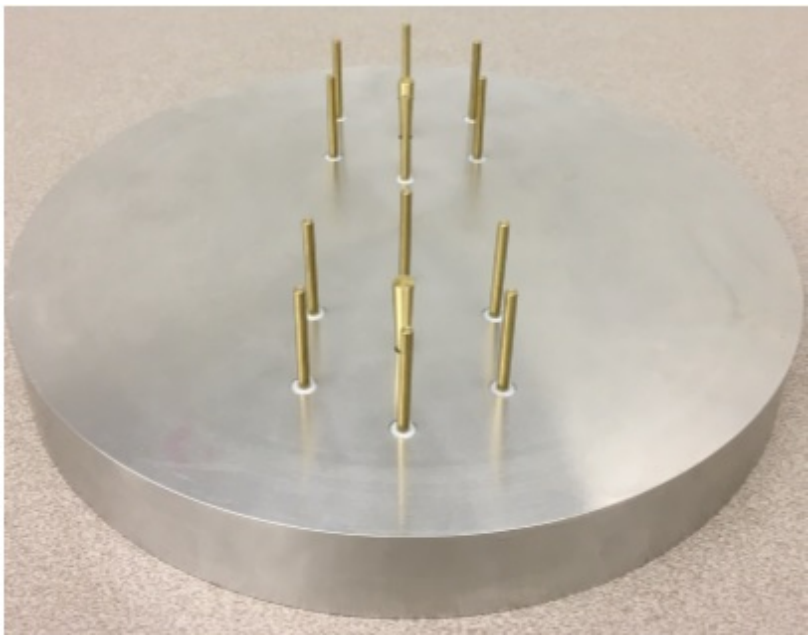

Figure 4.11: Fabricated antenna Model.

Parasitic elements are loaded with pin diodes, opening and shorting of pin diodes is regulated by the voltage from the field-programmable gate array (FPGA).

4.4 Mechanical Design

Monopole antenna elements are made from Copper with a 1.5 mm radius and these elements are threaded from the bottom. The ground plane is made up of Aluminum [36, 37].]. Aluminum ground plane reflects radio frequency waves. As a result, the antenna radiation pattern is slightly elevated [24, 38]. In order to add phase shift between currents of active elements, we are using a digital phase shifter from Macom, MAPS-011007. This phase shifter has a resolution of 5.6 degrees. The truth table for

the phase shifter is given in Table 4.2. Phase shifter evaluation kit and the FPGA setup is shown in Fig. 4.12.

Table 4.2: Truth Table for Phase Shifter

D6	D5	D4	D3	D2	D1	Phase Shift(degree)
0	0	0	0	0	1	5.6
0	0	0	0	1	0	11.2
0	0	0	1	0	0	22.5
0	0	1	0	0	0	45
0	1	0	0	0	0	90
1	0	0	0	0	0	180
1	1	1	1	1	1	354.4

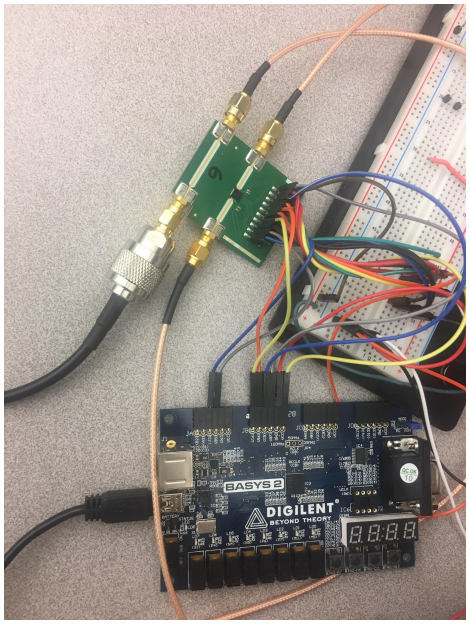

Figure 4.12: Simulated 7 element antenna Model.

The hollow skirted model, with the mounted PCB is shown in Fig. 5.11.

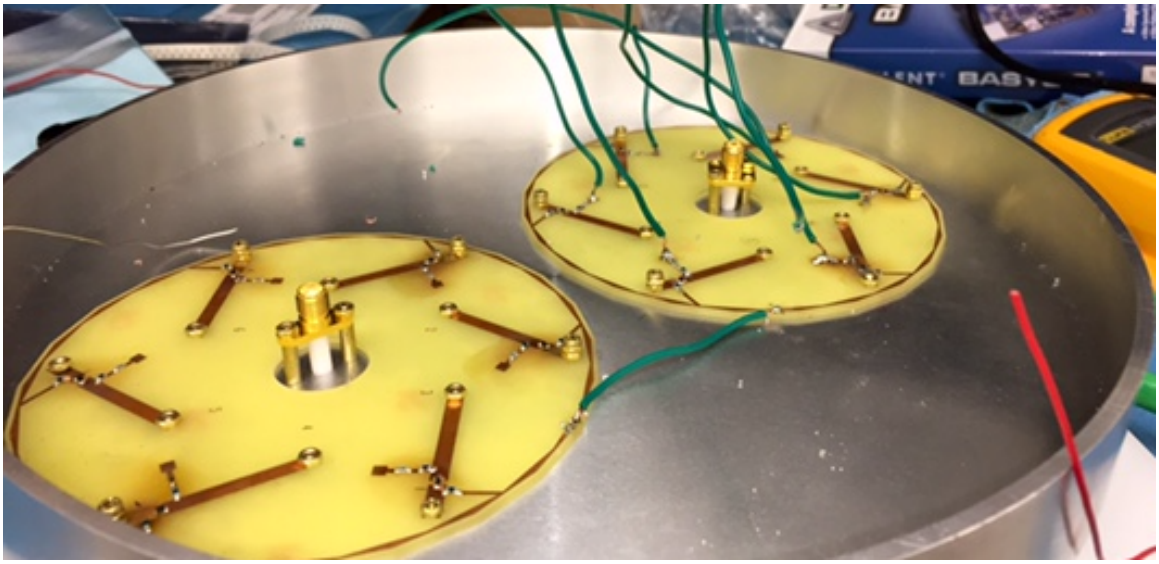

Figure 4.13: PCBs mounted at bottom of antenna.

4.5 Antenna Simulation and Hardware Results

As discussed previously, open elements act as directors and short elements act as reflectors [29]. Antenna beam is formed towards open elements and maximum gain is achieved in a direction where two adjacent elements of each array are open. For further beam steering, we have used the phase shifter between the active elements. Fig. 4.14 shows an overview of the simulated antenna. Element 1-1 (the first digit depicts array number and the second digit describes element number) is on the x-axis, for azimuth beam scanning we are considering x-axis as 0°. For maxima at 270°elements 1-5, 1-6, 2-5 and 2-6 are short and all other elements are open. Short elements are shown as black circles in Fig. 4.14. Radiation plot for gain at 270° is depicted in Fig. 4.15, where we can see that a gain of 11 dBi is achieved.

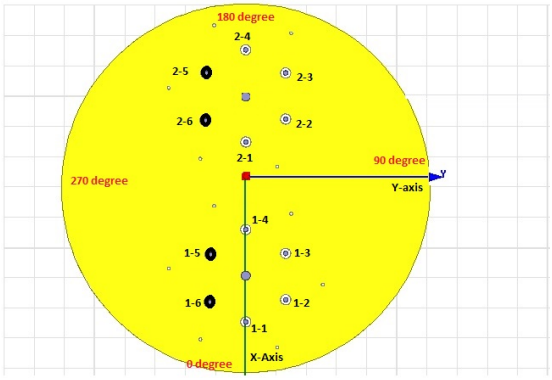

Figure 4.14: Simulated ESPAR Antenna with Elem 5 and 6 of Each Array as Open.

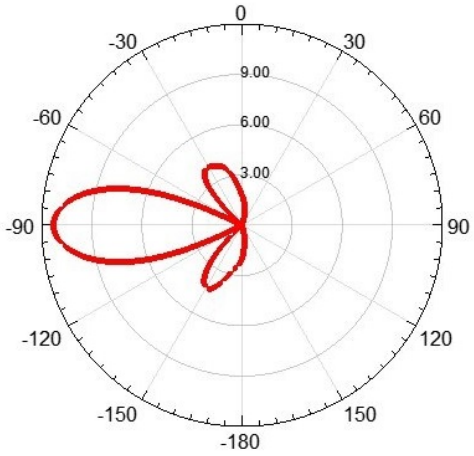

Figure 4.15: 2D plot for gain at 270°.

In order to further steer the beam, a phase shift of 50.4^0 is added. Fig. 4.16 shows a maxima at 265°. Here, we have added a phase difference of 50.4^0 between the two feed elements. Elements 1-5, 1-6, 2-5 and 2-6 are left open. We observe a maxima at 260° once a 72.8°phase shift is applied between the feed elements without changing the pin diode configuration. There is a side lobe of approximately 7 dBi in this case but the side lobe is 50° away from our intended direction. Fig. 4.17 shows a maximum simulated gain at 260°.

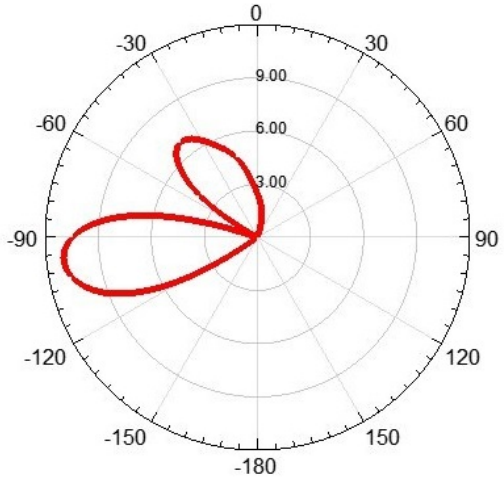

Figure 4.16: 2D plot for gain at 265^0.

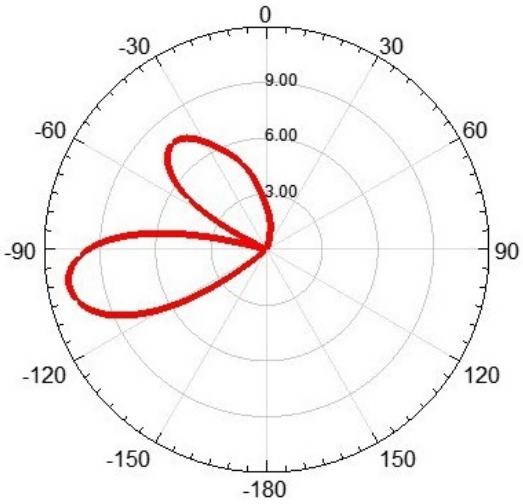

Figure 4.17: 2D plot for gain at 260^0.

The antenna elevation radiation pattern is elevated because the monopole elements are placed on an Aluminum ground plane. Fig. 4.18 shows a 2-D plot for elevation angle where we observe a maximum elevation angle of 68^0.

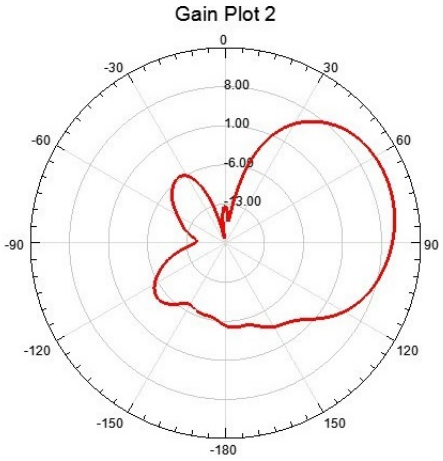

Figure 4.18: Elevation angle closer to 90 degrees.

Fig. 4.19 shows the bandwidth of the simulated antenna. We can observe that S_{11} is below -10 dB from 2.45 GHz - 2.62 GHz. Accordingly, the antenna has a bandwidth of 172 MHz and the bandwidth percentage is 6.9 %.

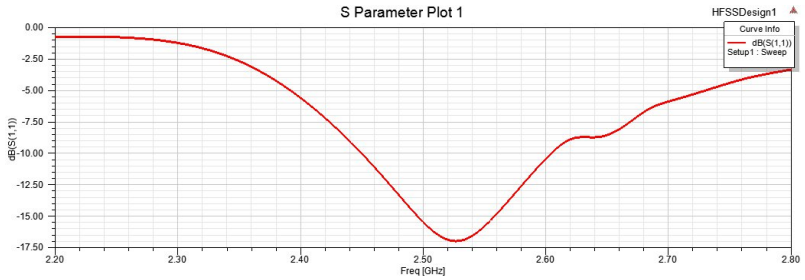

Figure 4.19: Bandwidth plot for Dual Array Antenna.

The simulated results are validated by hardware testing. The S_{11} plot of the fabricated antenna is obtained from VNA. In order to validate the antenna radiation pattern, we have performed the radiation pattern measurement in an anechoic chamber. The antenna has two active elements, input power to these elements is split equally by using an RF splitter. During testing, two horn antennas with known gains

were used to calculate path loss. Once we know P_t, P_r, G_r and path loss we can calculate, G_t by using Eriss Equation. P_r is given by:

$$P_r = P_t + G_t + G_r + Pathloss \tag{4.5}$$

$$G_t = P_r - P_t - G_r - Pathloss \tag{4.6}$$

Path loss is calculated as 56.5 dB by using the following equation:

$$Pathloss = P_r(26.5\,dBm) - P_t(0\,dBm) - G_r(16.5\,dB) - G_t(16.5\,dB) \tag{4.7}$$

Fig. 4.20 shows a plot for the radiation pattern at 270°. Here, elements 1-5, 1-6, 2-5 and 2-6 are short and there is no phase difference in excitation to feed elements. Hardware results are in line with the simulation results.

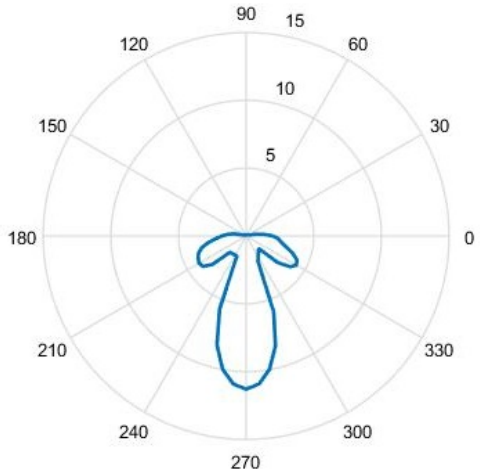

Figure 4.20: Hardware Results for maxima at 270 degree.

VNA measurements for S_{11} shows that antenna covers the frequency range from approx. 2.45 GHz - 2.59 GHz. The S_{11} plot for the antenna is in Fig. 4.21.

Figure 4.21: Bandwidth plot for Antenna Hardware.

All elements in conventional ESPAR antennas and switched parasitic array antennas are cylindrical. In our design the active element is conical. Antenna bandwidth has increased due to the tapered design of the active element. The S_{11} plot for the cylindrical central element is given in Fig. 4.22. Antenna bandwidth is 152 MHz.

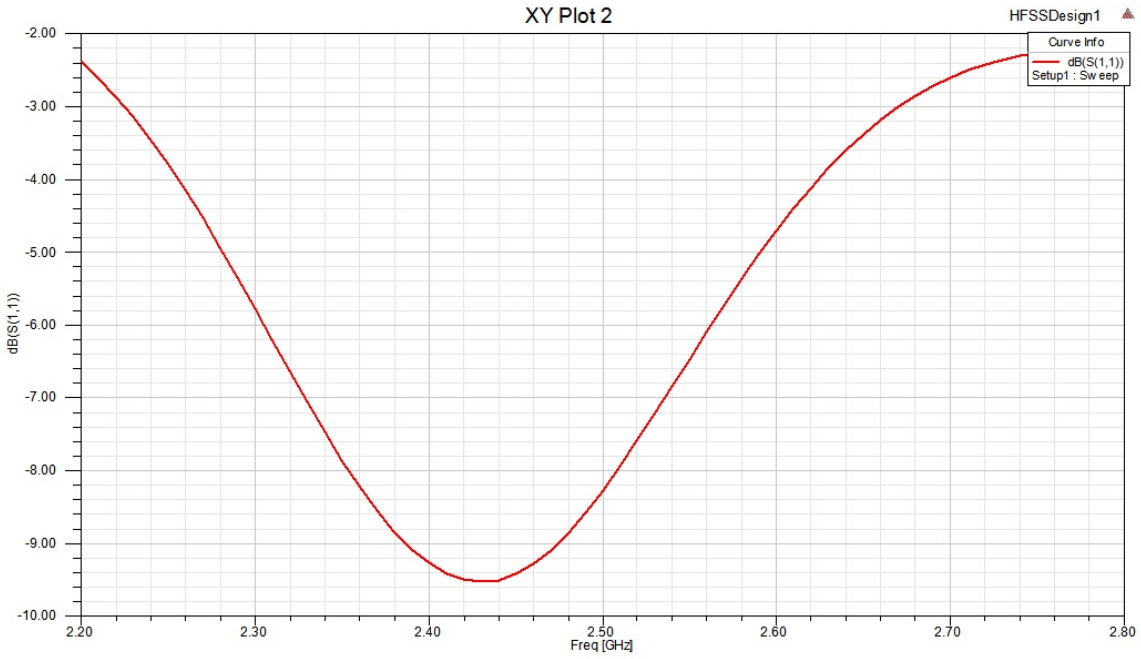

Figure 4.22: Cylindrical Monopole.

Fig. 4.23 shows the S_{11} plot for the center conical element. Antenna bandwidth is 190 MHz. Antenna bandwidth has improved in comparison to conventional ESPAR antenna due to the tapered design of the active elements.

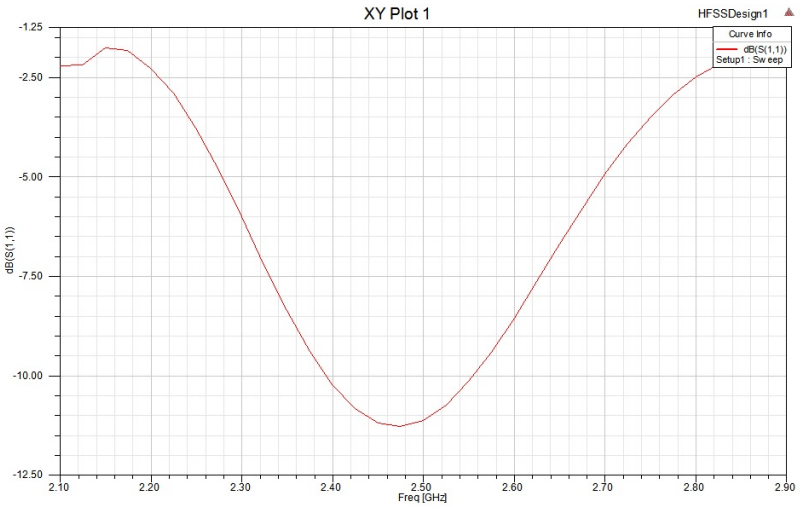

Figure 4.23: Conical Monopole.

Fig. 4.24 shows the S_{11} plot for variable lengths from 27 mm to 34 mm in steps of 1 mm. We note that the length of 30 mm is optimum.

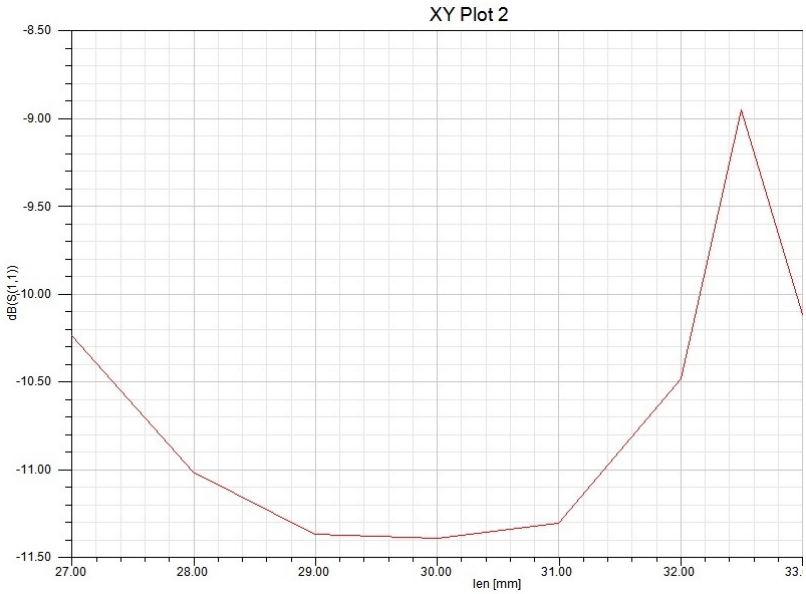

Figure 4.24: Element length optimization.

4.6 Formation of Dual Beam with Single RF Chain

One of the most significant advantages of the designed antenna is that it can support up to 3 steerable beams by using a single RF chain. Multiple beams can help to increase spatial diversity in wireless systems. We have additional beams without increasing feed losses (single RF chain is used). Fig. 4.25 shows the two beams that are formed at +45 degree and -45 degree. Here, element 1 of array one is open. Elements 1, 2 and 6 are open for array 2, the phase difference between excitation currents is 120 degrees.

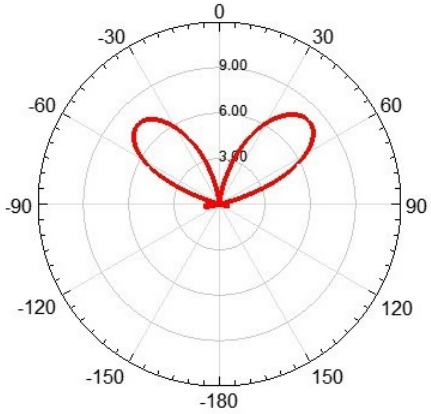

Figure 4.25: Maxima at +45 and -45 degrees.

Fig. 4.26 shows the formation of dual beams at +50 and -50 degrees. Here, we have kept element 1 of the array one open. Elements 1, 2 and 6 of the array two are open. The phase difference between excitation currents is increased to 150 degrees.

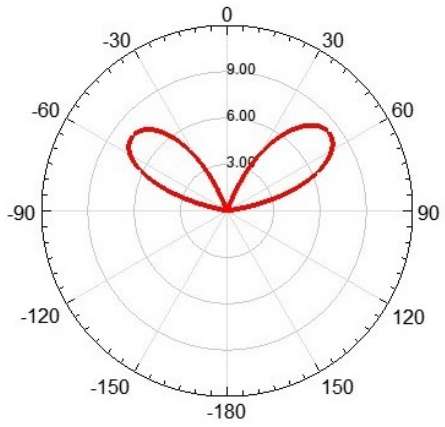

Figure 4.26: Maxima at +50 and -50 degrees.

Fig. 4.27 shows the formation of dual beams at +60 and -60 degrees. Here, we have kept element 1 of the array one open. Elements 1, 2 and 6 of the array two are open. The phase difference between excitation currents is increased to 180 degrees.

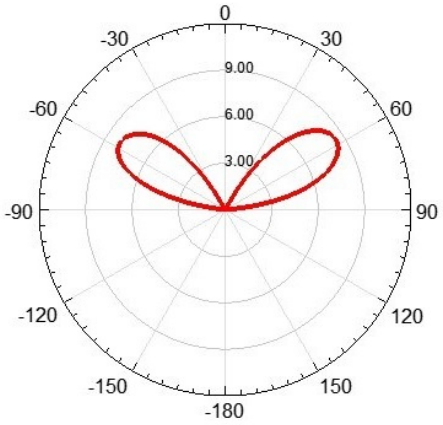

Figure 4.27: Maxima at +60 and -60 degrees.

Fig. 4.28 shows the formation of dual beams at +65 and -65 degrees. Here, we have kept element 1 of the array one open. Elements 1, 2 and 6 of the array two are open. The phase difference between excitation currents is increased to 220 degrees.

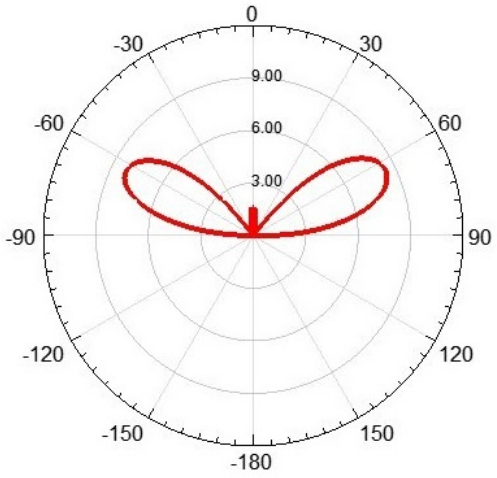

Figure 4.28: Maxima at +65 and -65 degrees.

The 3D polar plot for dual beamforming is shown in Fig. 4.29. Here, we can see the formation of two beams.

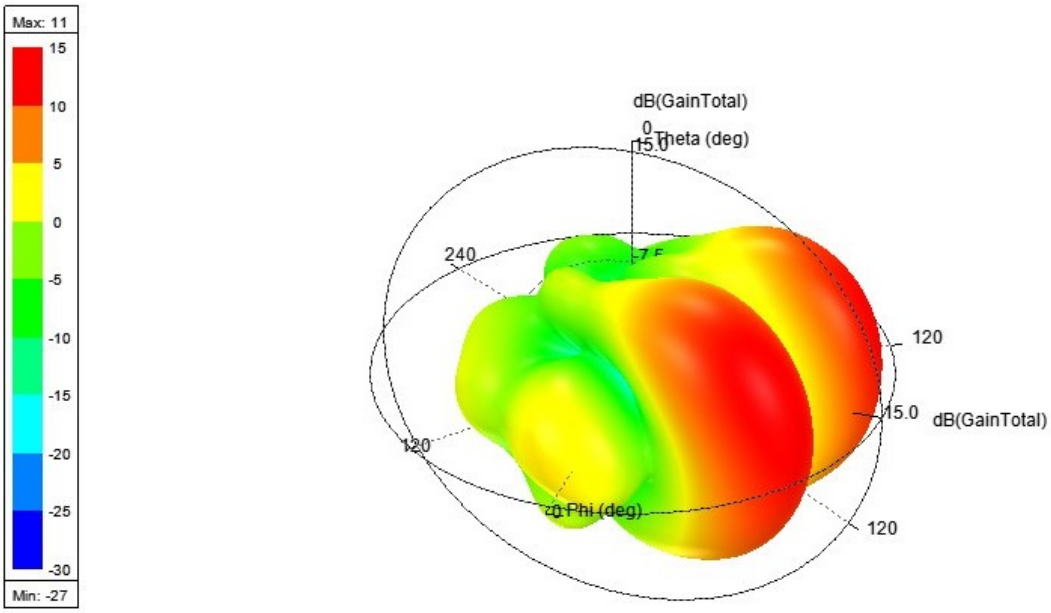

Figure 4.29: 3-D Polar Plot for Dual Beam

CHAPTER 5

KA BAND ANTENNA DESIGN

The millimeter wave (mm-Wave) band ranges from 30 GHz - 300 GHz. This frequency spectrum has garnered significant attention due to the high data rate requirements of the next generation of wireless networks, i.e., 5G. In fact, it is expected that 5G will support peak data rates of 20 Gigabits per second (Gbps). Due to lack of free bandwidth at lower frequencies, the mm-Waves band is considered as a potential band for the rollout of 5G services. To this end, the FCC has opened 10.85 GHz of spectrum for potential 5G applications in frequency ranges beyond 24 GHz [1]. The specific bands available for communication are::

- 27.5 GHz - 28.35 GHz (0.85 GHz bandwidth)
- 37GHz - 40 GHz (3 GHz bandwidth)
- 64-71 GHz (7 GHz bandwidth)

The frequency band from 27.5 GHz - 28.35 GHz and from 37 GHz - 40 GHz is licensed, whereas the frequency band from 64 GHz - 71 GHz is unlicensed [39]. The Unlicensed frequency band is adjacent to the ISM band from 57 GHz - 64 GHz. In total, there is 14 GHz of unlicensed bandwidth available from 57 GHz - 71 GHz. The advantages of mm-Wave communication are as follows:

- There is the availability of sufficient free bandwidth in the mm-Wave frequency band to support high data rates.

- Antennas for the mm-Wave band are small in dimension. This makes the integration of smart beam-steering antennas with mobile devices more practical.

- mm-Wave signals travel shorter distances and do not penetrate solid objects. This makes mm-wave frequency reuse easy in densely packed cell sites.

However, aside from the above advantages, there are a handful of challenges which need to be addressed to make mm-Wave communication possible. High atmospheric absorption and free space loss are most prominent challenges for mm-Wave communication. Free space loss is dependent on the distance between the transmit and the receive antennas, for isotropic antenna free space loss is given as [40]:

$$FSL = \frac{4\pi R}{\lambda^2} \tag{5.1}$$

$$FSL_{dB} = 92.4 + 20logF + 20logR \tag{5.2}$$

Here, R is the distance between the transmit (Tx) and the receive (Rx) antennas and F is the frequency of operation. Based on equation (5.2), by doubling the distances between Tx and Rx antennas, attenuation is increased by 6 dB [41]. Due to high path loss, mm-Wave communication has a limited range. Significant contributors to signal attenuation at mm-Wave frequencies are covered in the following sub-sections.

5.0.1 Losses Due to Atmospheric Gases

mm-Wave signals are prone to losses due to absorption by oxygen molecules, water vapors, and other atmospheric gases. Atmospheric losses are greater when mm-Wave frequency matches with the resonant frequency of atmospheric gases. At 24 GHz atmospheric attenuation is high due to the absorption of the mm-Wave signals by the water molecules. At 60 GHz atmospheric absorption is high due to the absorption of mm-Wave signals by oxygen molecules. Fig. 5.1 shows the dB/km of attenuation due to the atmospheric gases and molecules [42]. In Fig. 5.1, we can see that attenuation is high at 24 GHz and 60 GHz. Moreover, one can also notice that atmospheric attenuation increases with frequency [43].

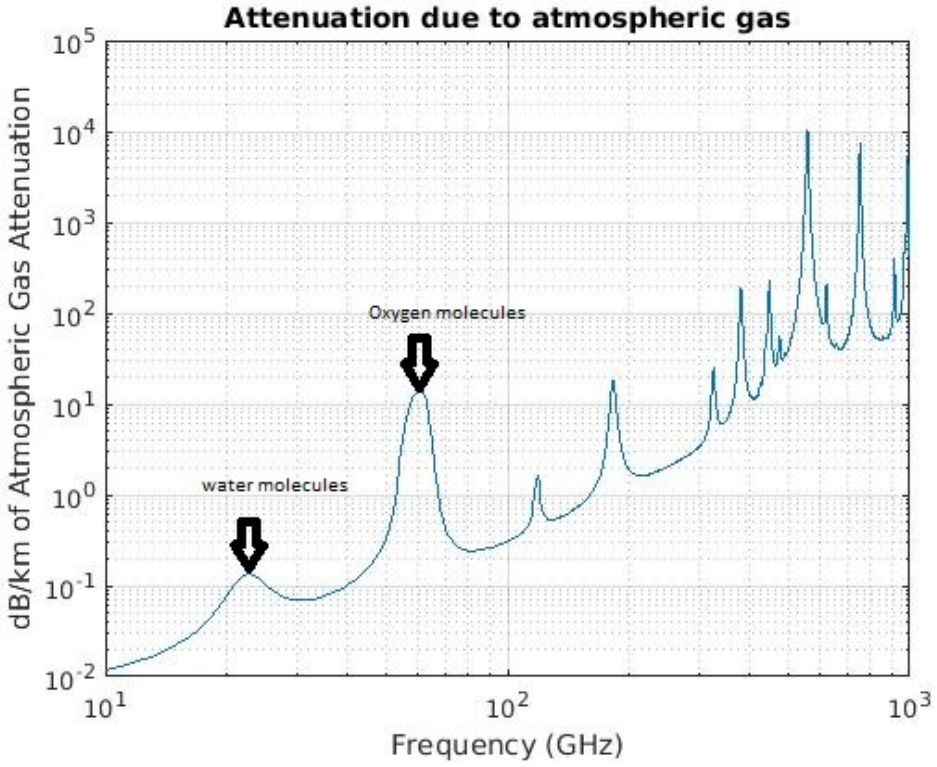

Figure 5.1: Attenuation due to atmospheric gases.

5.0.2 Rain Losses

Losses due to the rain is another factor which restricts the range of mm-Wave signals. Size of raindrops is comparable with the wavelength of RF waves, especially around 100 GHz. This causes scattering of RF due to raindrops. Fig. 5.2 shows the rain attenuation for 1mm/hr, 4 mm/hr, 8 mm/hr and 16 mm/hr of rain rate. As rain rate (mm/hr) increases rain attenuation also increases due to the higher rate of scattering of RF waves by raindrops [42].

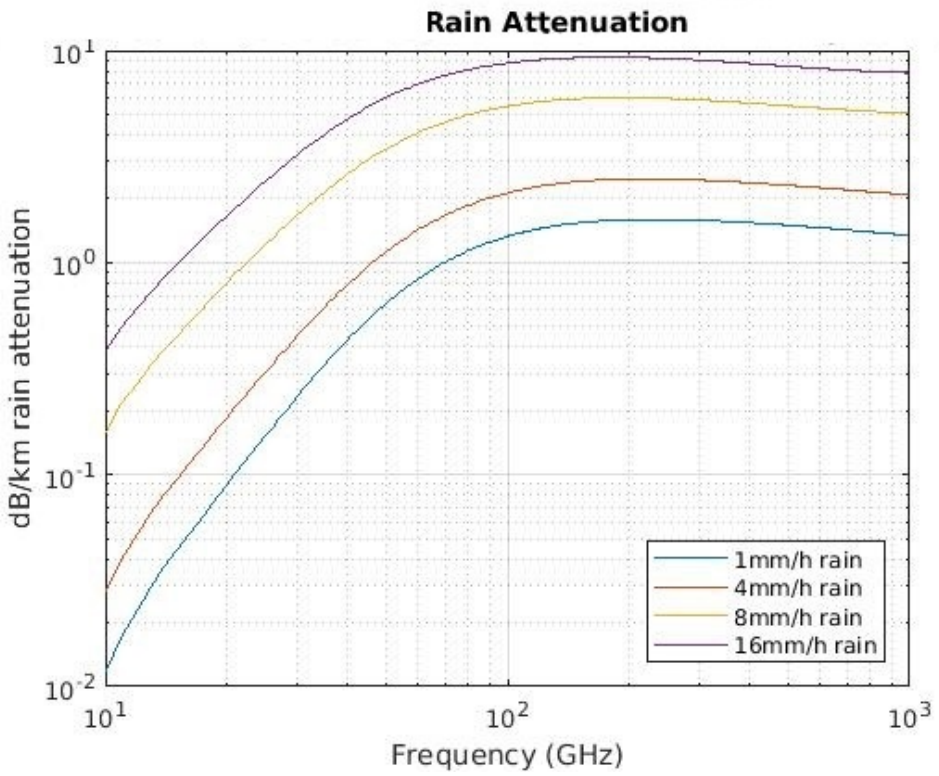

Figure 5.2: Rain Attenuation Model.

5.0.3 Losses Due to Fog / Cloud

For frequencies higher than 10 GHz, there is considerable attenuation due to fog and clouds. The fog attenuation should be accounted in link budget analysis,

especially at mm-Wave frequencies. Fig. 5.3 shows the fog attenuation in dB/km for frequencies between 10 GHz to 1000 GHz [42].

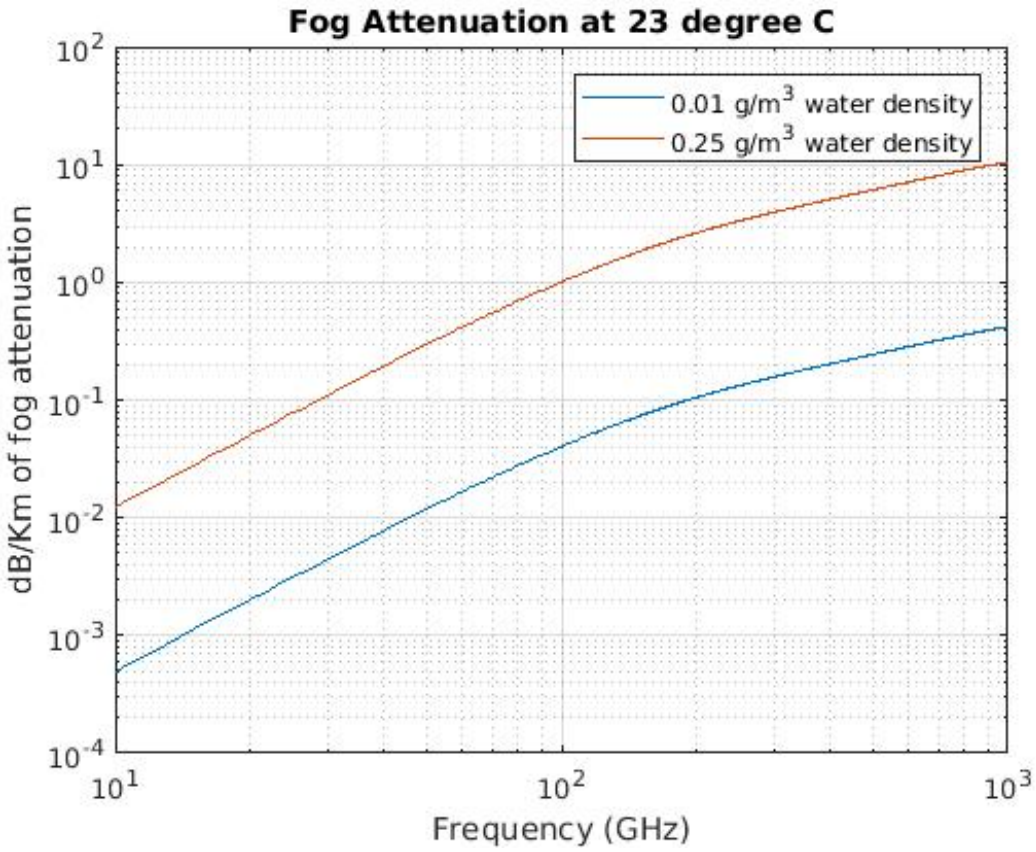

Figure 5.3: Fog Attenuation.

The total path loss for 60 GHz radar is given in Fig. 5.4, from these results, it is clear that at 60 GHz atmospheric attenuation is significantly higher due to absorption of RF waves by oxygen molecules. At a distance of 400 m attenuation due to atmospheric gases is 10 dB. Total path loss at 400 m for 60 GHz radar is close to 105 dB [42].

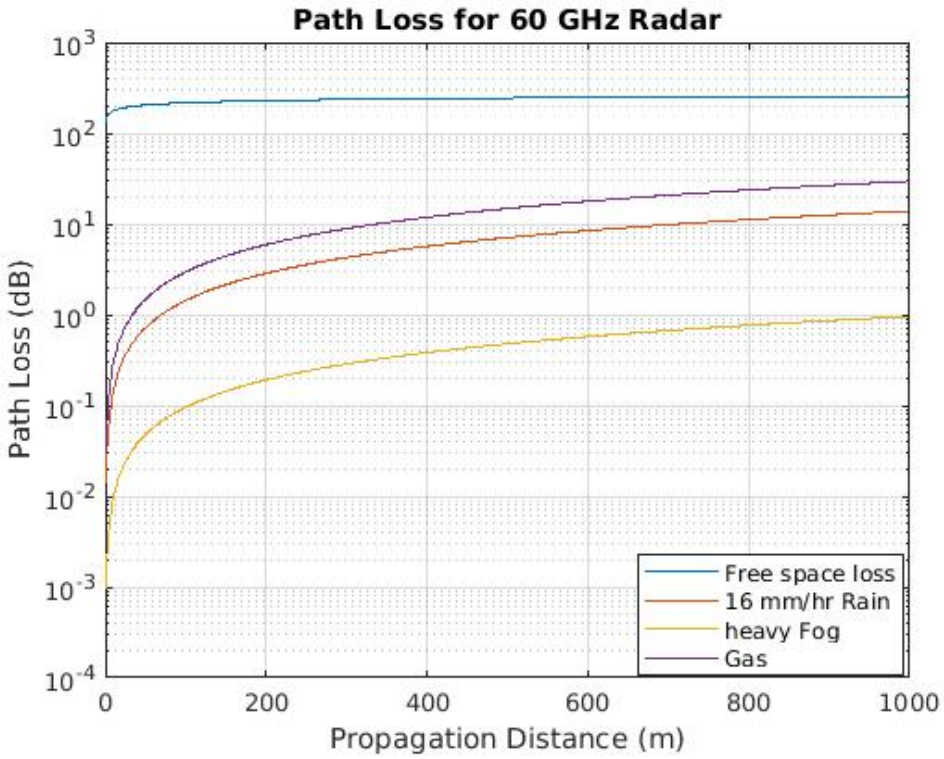

Figure 5.4: Total Path Loss at 60 GHz.

5.1 Smart Antenna for mmWave communication

From above, it is evident that at mm-Wave frequencies overall path loss is high due to multiple factors. In order to account for this high path loss, smart antennas and advanced digital signal processing techniques shall be used in mm-Wave communication systems. We have designed a smart antenna with the center frequency of 28 GHz for 5G and mm-Wave communication systems. The proposed smart antenna uses a hybrid of phased array and parasitic array approach for beam-steering. This methodology is based on our recently approved patent. Antenna design consists of two circular arrays of passive elements on a single ground plane. Each circular array has an active element at its center. By varying the phase of the current in the active and

passive elements, beam steering is achieved. In our design, a phase shifter is added to introduce a phase shift between excitation currents of active elements. Open elements have capacitive reactance and behave as directors, whereas short elements behave as reflectors [26, 23]. Total electric field $E(\phi)_{tot}$ is expressed as:

$$E(\phi)_{tot} = E(\phi)_{elem} \times A.F(ArrayFactor) \tag{5.3}$$

Here $E(\phi)_{elem}$ is the electric field of an individual element and A.F is array factor. Array factor of the designed antenna is expressed as [21]:

$$A.F = \sum_{m=0}^{M} l_m(\theta) i_m a_m(\theta, \phi) e^{j\gamma} \tag{5.4}$$

where $l_m(\theta)$ is the vector effective length, i_m is the port current and $a_m(\theta, \phi)$ is the steering vector. γ is the phase difference between the excitation currents of active elements. By combining equations (8.3) and (8.4), $E(\phi)_{tot}$ is expressed as [23]:

$$E(\phi)_{tot} = j\frac{Z_0}{2\lambda}\frac{e^{-jr}}{r}\sum_{m=0}^{M} l_m(\theta) i_m a_m(\theta, \phi) e^{j\gamma} \tag{5.5}$$

Our design involves a two-dimensional array of parasitic elements, steering vector $a_m(\theta, \phi)$ depends on x and y coordinates of each element and it is expressed as:

$$a_m(\theta, \phi) = \sum_{m=1}^{M} e^{jk(\sin(\theta)\cos(\phi)x_m + \sin(\theta)\sin(\phi)y_m)} \tag{5.6}$$

where $l_m(\theta)$ is the vector effective length. Vector effective length is used to determine the induced open circuit voltage when waves impinge on an antenna. The vector effective length is given by [26, 23]:

$$l_m = l_m^0(1 - \alpha_m x_m) \tag{5.7}$$

Here, l_m^0 and α_m are structural parameters and depend on the design. From the equation (8.5), it can be deduced that by varying port current i_m net electric field is varied. Induced port current is dependent on the reactance of each parasitic element and the expression for the port current is given by:

$$I = (Z_{mn} + X)^{-1} V_s \tag{5.8}$$

Here, X is the reactance matrix. By varying the reactance of each element, the total electric field is varied and the antenna beam is steered, X is determined as [27]:

$$X = diag[z_0, jx_1, jx_2, jx_3, jx_4, jx_5, jx_6...] \tag{5.9}$$

In our proposed mathematical model, the beam is steered by:

- Opening and shorting a sequence of the parasitic elements.
- By varying the phase difference between the excitation current of active elements.

The proposed novel methodology exploits the advantages of both phased and parasitic array approaches. The proposed design has the following advantages over traditional smart antennas:

- Antenna size is small as compared to phased array antennas, since the parasitic elements exploit the mutual coupling amongst antenna elements. This allows the antenna elements to be placed $\lambda/4$ apart from each other, which results in the compact size antenna.

- Only one phase shifter is used in our design. As a result, the antenna is low cost and simple to manufacture as compared to phased array antennas. In phased array antennas, each antenna element has a phased shifter at its input for beam-steering.

- The design is simple and easy to implement as compared to ESPAR antennas. We have used simple, low-cost RF switches for beam-steering

5.2 Antenna Simulation and Design Parameters

For validation of the proposed technique, we have simulated the antenna in Ansoft HFSS. Antenna design consists of two circular arrays on top of the ground plane. Each circular array has six parasitic and one active monopole element. For simulating the opening and shorting of parasitic elements we are changing the resistance of the lumped RLC boundary in HFSS. Material for ground plane is selected as Aluminum and material for the parasitic elements is selected as Copper. Antenna design parameters are shown in Table 5.1.

Table 5.1: Design Parameters

Parameters	Values
Ground Skirt Length	7.8 mm
Monopole Length	2.19 mm
Frequency	28 GHz
Wavelength	10.71 mm
Distance between monopoles	3.7 mm
Ground Thickness	3mm

5.2.1 Simulation Results

Due to mechanical design constraints, we have increased the separation distance between elements to λ/2.9 (3.7 mm) instead of λ/4 (2.667 mm) due to which sidelobe levels are relatively high and the beam is less directional as compared to the design with the separation distance of λ/4 (2.667 mm). Simulated antenna model is shown in Fig. 5.5.

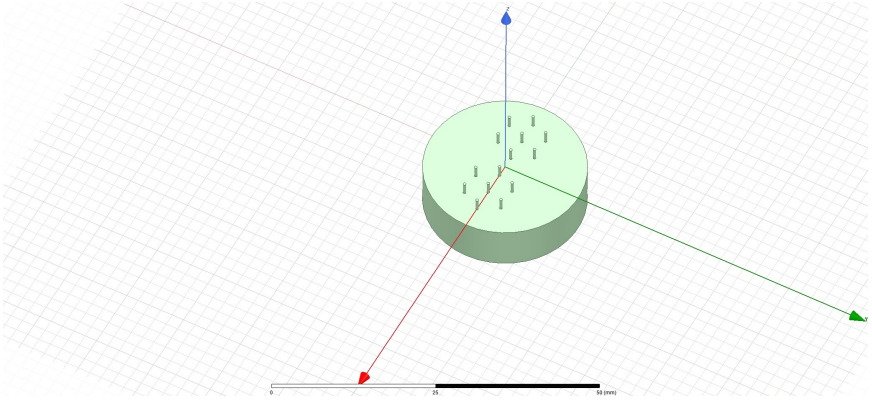

Figure 5.5: Simulated antenna Model.

Antenna bandwidth is optimized by simulating multiple lengths of monopole elements. At a length of 2.196 mm, optimal bandwidth is achieved for 28 GHz. The S11 plot for multiple lengths of monopole elements is shown in Fig. 5.6.

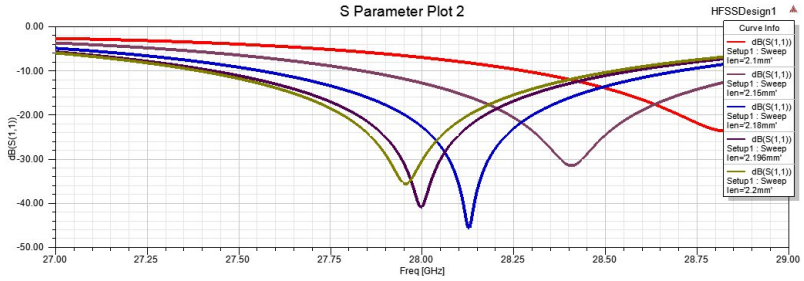

Figure 5.6: Length Optimization.

The S_{11} plot with the monopole length of 2.196 is shown in Fig. 5.7. From Fig. 5.7 it can be seen that the simulated antenna has a bandwidth of 1.18 GHz.

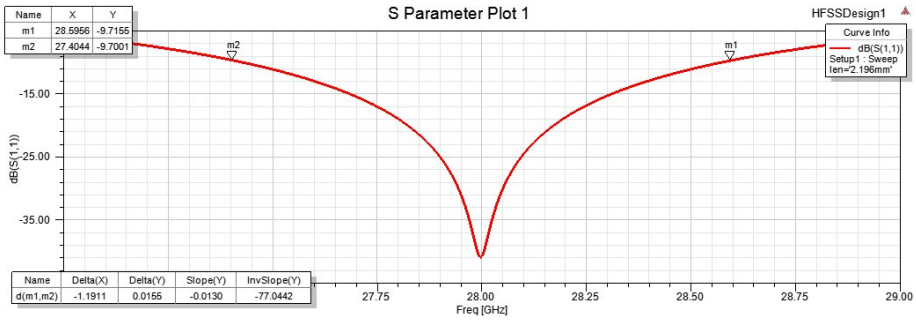

Figure 5.7: S_{11} plot.

By opening elements 5 and 6 of both array and shorting all other elements, the main beam is formed at 270^0. This is shown in Fig. 5.8.

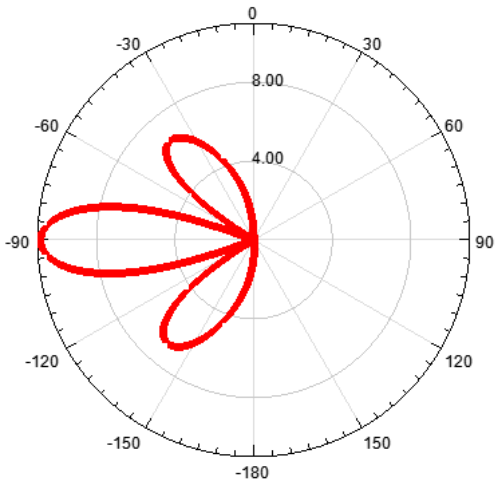

Figure 5.8: Maxima at 270^0.

By keeping elements 5 and 6 of each array open and adding a phase difference of 30^0 between the excitation currents of the feed elements, the main radiation lobe is formed at 265^0 as shown in Fig. 5.9.

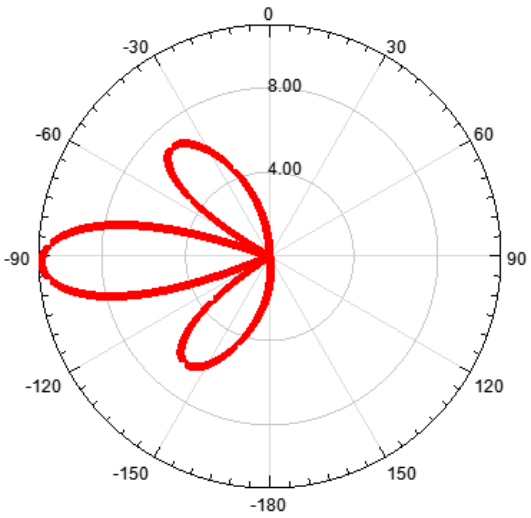

Figure 5.9: Maxima at 265^0

Fig. 5.10 shows the simulated results when passive elements 3, 4 and 5 on both arrays are left open while the remaining elements are shorted. A gain of approximately 7 dBi is achieved on two beams, and the third beam has a gain of 5 dBi.

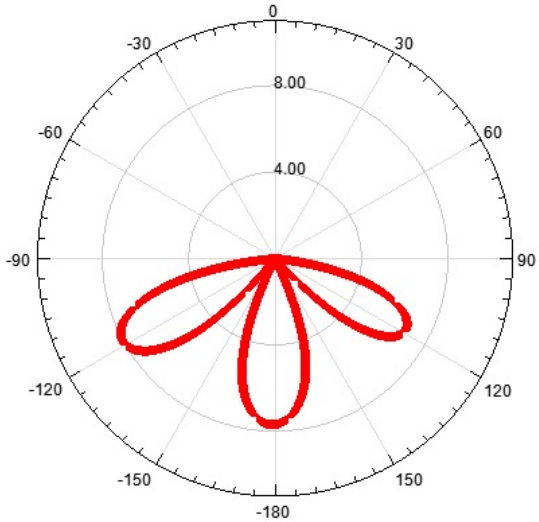

Figure 5.10: Formation of three beams.

5.2.2 Hardware Results

Subsequent to successful antenna simulations, we fabricated the proposed antenna. Opening and shorting of parasitic elements is controlled by using mechanical shorts due to the expenses associated with RF switches at mm-Wave frequencies. Simulation and hardware results are for center frequency of 28.5 GHz.

Figure 5.11: Fabricated Antenna.

S_{11} plot is shown in Fig. 5.12. S_{11} plot differs slightly from simulation due to the presence of the power divider but follows the same pattern as simulations.

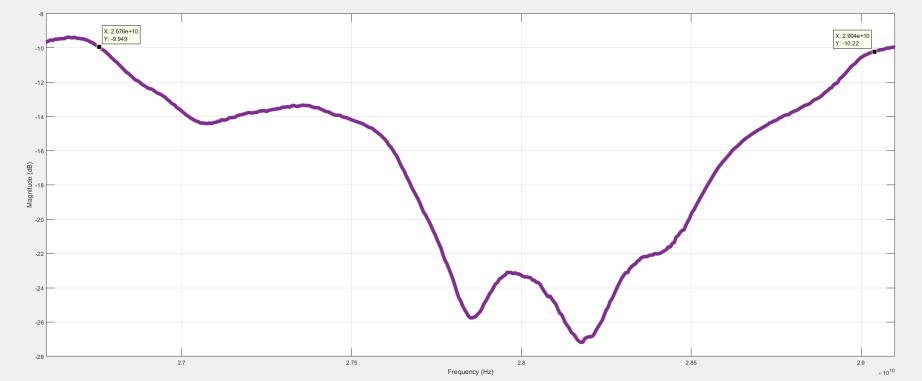

Figure 5.12: S_{11} measured from VNA.

CHAPTER 6

SATELLITE COMMUNICATION AND ADAPTIVE BEAMFORMING ANTENNAS

6.1 Satellite Communication

There are three basic components of a satellite communication system, the transmit earth station, the satellite (space segment) and the receive earth station. Telecommunication satellites are satellites that receive a signal from the ground segment (remote terminal or hub station), amplify the received signal and then re-transmit it back to the ground segment (remote terminal or hub station). Communication satellites basically relay the signal between any two points. Bent-pipe satellites are those satellites which do not process the received signals and simply reflect it back to the earth without processing, whereas onboard processing satellites are the satellites which process the received signals. A few common types of satellites are:

- Communication Satellites
- Navigational Satellites
- Remote Sensing Satellites
- Weather Satellites

The link from the transmit earth station to the satellite is called the uplink, whereas the link from the receive earth station to the ground is called the downlink. Uplink has a higher frequency as compared to the downlink. Higher frequencies suffer more attenuation and require higher transmit power. The ground segment has ample power as compared to the space segment where mainly solar panels power satellites. Therefore, higher frequencies are allocated for the uplink and the lower frequencies are allocated for the downlink (see Fig. 6.1). Low noise block (LNB) amplifies and down-converts the received signals, whereas block up converter (BUC) amplifies and upconverts the signal received from modem / Hub chassis.

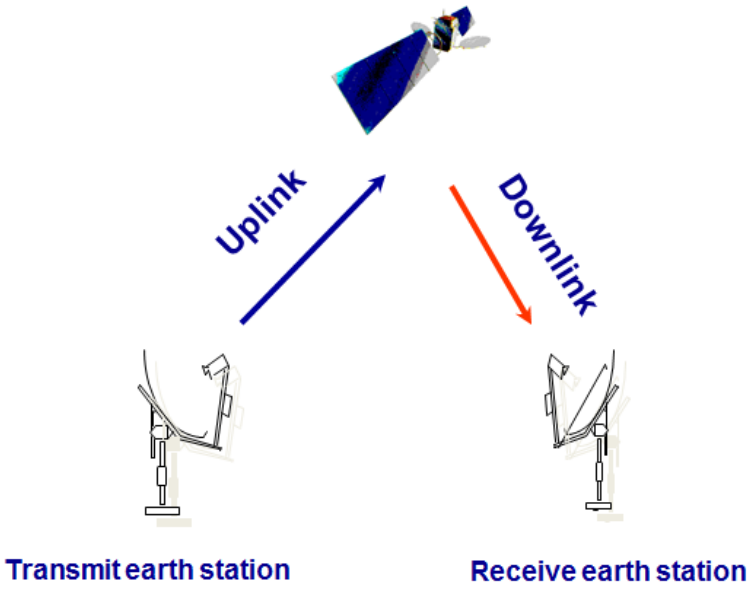

Figure 6.1: Uplink Vs. Downlink frequency Satellite.

Commercial satellite communication systems operate in three bands:

- C-band (ranges from 4 - 8 GHz)
- Ku-band (ranges from 12- 18 GHz)

- Ka-band (Ranges from 26 - 40 GHz)

Satellites revolve around the earth in fixed orbits Table 6.1 [44] shows the different radii used for satellite positioning.

Table 6.1: Satellite Orbits

Parameters	Leo	Meo	Geo
Path Loss	low	high	high
Orbital Period	10-40 minutes	2-8 hr	24 hr
No of Satellite for global coverage	40 minimum	8 minimum	3 minimum
Height	500-1500 km	5000-12000 km	36,000 km

Satellite communication links have an inherent delay of around 480 ms. This large delay has been one of the drawbacks of satellite communications for delay sensitive applications.

6.2 Types of Terminals

In the following subsections, we have the following forms of the ground terminals:

6.2.1 Fixed Terminals

Fixed terminals are the type of ground terminals which have a fixed location. e.g., ATMs, teleport stations, etc.

6.2.2 Communication On The Pause Terminals

These are the terminals which are mobile but do not transmit or receive when the terminal is on the move, e.g., DSNG media vehicles.

6.2.3 Communication On The Move Terminals

Communication on the move terminals transmits and receives RF signals while terminals are on the move. e.g., airborne commercial flights.

6.3 Beam Steering Antennas for Satellite Communication

There are different platforms for satellite communication available in the market. Commonly used platforms are as follows:

- Hughes
- iDirect
- ComTech
- Viasat
- Gilat

In Hub based platforms, there is a centrally shared carrier which is uplinked from the teleport station. All remote terminals receive the shared carrier (downstream). For airborne satellite communication, the remote terminals are airborne [45, 46]. Antenna beam has to point towards the satellite. The beam can be steered mechanically as well as electronically. For Ku systems mechanical beam-steering approach is used, 2Ku systems also use mechanical beam-steering. As mechanical beam steering involves moving parts, it requires more power, and it is prone to wear and tear. Antenna systems supporting satellite communication, especially airborne communication, shall constantly be analyzed for performance and optimization. Satellites are placed along the equator. However, once airborne terminals fly near the equator, the elevation

angle reaches a high value. Due to the large elevation angle, antennas may not be able to keep track of satellite communication signals [47]. At this point, performance analysis is critical to determine what changes can be further made to enhance the elevation angle and maintain satellite communication links.

6.4 Beam Switch Time and Data Analysis

With the advent of high-density satellites, analyzing and verifying the system performance, and replacing the poorly performing system components has become increasingly important. Monitoring requirements shall be defined and understood. Research is going on the following critical topics:

- Analysis of the maximum elevation angle of the deployed antenna, and subsequently modifying the frequency of operations or the network to combat degradation at high elevation angles.
- Analysis of beam-switching delay between beams. This analysis is important if the delay is more than a certain threshold, the satellite communication link will be lost. Therefore, research to accurately measure beam switching delay is an active research topic.
- The trade-off between modulation schemes versus bandwidth usage and datarate measurement.
- The application of forward error correction schemes versus bandwidth efficiency.

In order to maintain satellite communication link, optimal wireless performance is required. For higher modulation and higher forward error correction (FEC) rates, the signal to noise ratio shall be higher. In case of iDirect, the signal to noise of 10

dB is optimal for quadrature phase shift keying (QPSK). For binary phase shift keying (BPSK) the optimal signal to noise ratio is 7dB [48]. The concept of satellite links supporting airborne application is depicted in Fig. 6.2 and the concept of airborne communication using the terrestrial networks demonstrated in Fig. 6.3.

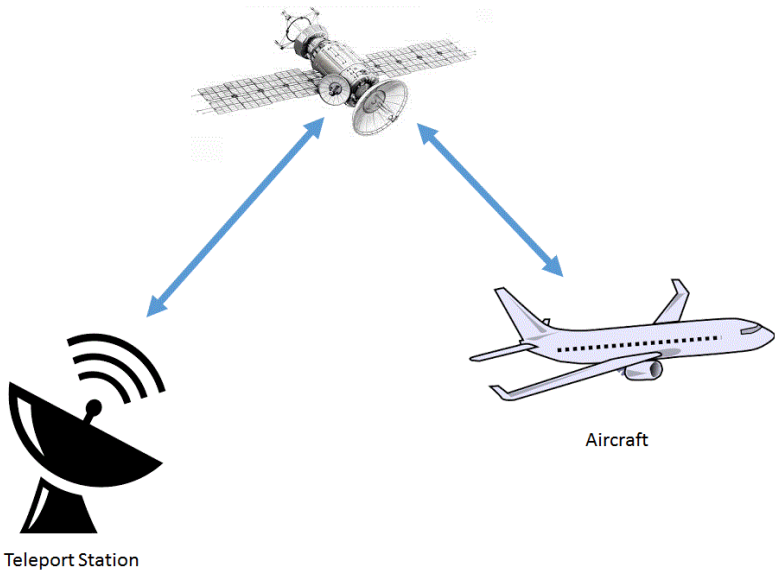

Figure 6.2: Commercial internet using satellite communication.

The following tasks that were undertaken at a leading satellite communication company for commercial aviation applications formed the basis of the dissertation:

- Root cause analysis of poorly performing Ku band satellite communication links.
- Identification of latency and ping loss in satellite communication links.
- Analysis of SNR vs. modulation schemes and satellite bandwidth usage.
- Beam steering and signal tracking analysis of 2Ku satellite communication antenna systems.

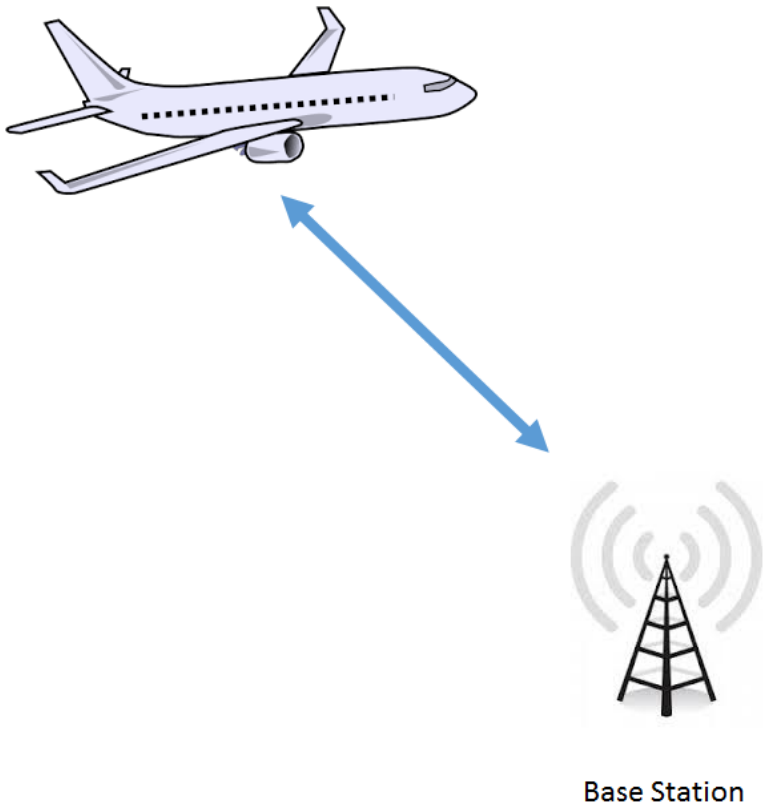

Figure 6.3: Commercial Internet using Terrestrial Networks.

- Performance characterization of beam-steering satellite communication antennas.

6.5 Beam Steering Mechanisms Available in Market

6.5.1 Mechanical Beam Steering Antenna

For satellite communication in commercial aviation mechanical beam-steering antennas are used more often than electronic beam-steering antennas due to cost. Reflector-based antennas are not recommended for use in commercial aviation industry due to their high profile design. Instead of reflector/parabolic antennas, flat

panel antennas are used. Such antennas are common due to their low profile design. The gain of flat panel antennas is not high. Therefore, such antennas are often used in conjunction with spread spectrum techniques. Variable Inclination Continuous Transverse Stub (VICTS) is another form of mechanical beam-steering antennas. In VICTS, beam-steering is accomplished by relative movement of antenna platters. Differential movement of platters varies polarization and the elevation angle of the antenna while common movement of platters varies the azimuth angle of the antenna.

6.5.2 Phased Array Antennas (Electronic Beamsteering)

Phased array antennas are also used for satellite communication. Fig. 6.4 shows a phased array antenna design. Such antennas are not commonly used in commercial aviation due to the following drawbacks:

- Phased array antennas can not work at low elevation angles.
- Phased array antennas have a high cost of implementation.

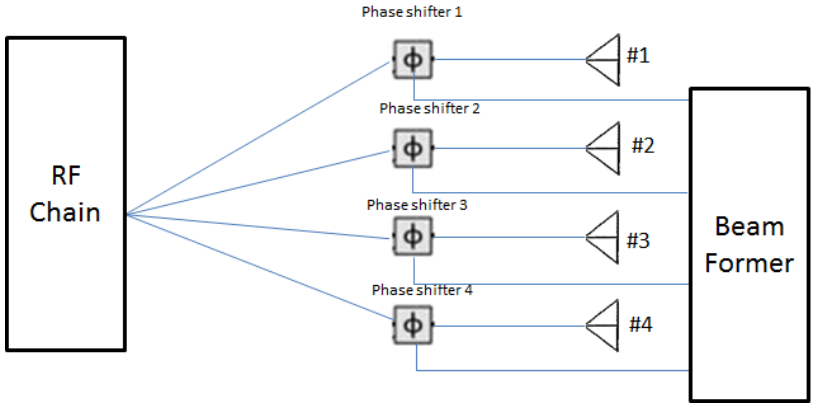

Figure 6.4: Phased Array Antenna.

6.5.3 Metamaterial Antennas (Electronic Beamsteering)

Electronic beam-steering can also be achieved by using metamaterial antennas. Metamaterial antenna technology involves selection and deselection of thousands of metamaterial elements. Element design is based on liquid crystals and RF waves are radiated from each element once it is activated. By varying combination of active (selected) elements, the beam is steered.

6.6 Cube Satellites

Cube satellites are low-cost satellites with small dimensions. The size of a cube satellite can be as small as a book. Cube satellite constellations are proposed by SpaceX, Telesat and OneWeb. Constellations of cube satellites operating at Ku and Ka band will be placed in LEO in the near future. Because of low latency cube satellites can work as an alternative for providing broadband internet to remote regions. Approved cubes satellite constellations for various companies are [49] as follows:

- 720 satellites are approved by the FCC for OneWeb. Another 1260 satellites are recently approved. In total OneWeb will have 1980 satellites in LEO band operating at Ku and Ka frequency.
- SpaceX has the FCC approval for 4425 cube satellites.
- Telesat has the FCC approval for 118 cube satellites, one cube satellite for Telesat is already in LEO for testing purposes, the satellite was launched in Jan. 2018 by the Indian Space Research Organization (ISRO).

Cube Satellites can be classified into the following categories:

- Mini-satellite (110–700 kg approximately)
- Micro-satellite (11–110 kg approximately)
- Nano-satellite (3–11 kg approximately)
- Pico-satellite (0.3–3 kg approximately)
- Femto-satellite (0.03–0.3 kg approximately)

Conceptually cube satellites are made of Software Defined Radios (SDRs). Hence, these systems can be easily upgraded to the latest technology available in the market [50]. Research challenges in cube satellite communication are:

- Satellites will be moving at considerable speed. Ground tracking antennas will have to be robust for tracking cube satellites.
- Deployment of an antenna for cube satellites is challenging. One has to design high gain antennas over a small surface area.
- Cube satellite design involves Software Defined Radios (SDRs), which makes the design complex and requires significant power consumption.

CHAPTER 7

CONCLUSION AND FUTURE WORK

7.1 Conclusion

We have proposed and designed a hybrid phase and the parasitic array antenna. The designed antenna is capable of supporting multiple radiation patterns (up to 3). First, the mathematical modeling of the proposed antenna was completed. Subsequently, the antenna was designed in HFSS. Two antennas are designed for separate frequency ranges. The first antenna is centered at 2.5 GHz, and its maximum gain is close to 11 dBi for one beam. For two beams the antenna gain is close to 8 dBi (each beam has a gain of 8 dBi). Antenna beam is steered by:

- Varying the phase of excitation currents between active elements.

- Opening and shorting sequence of the parasitic elements.

After proof of concept at 2.5 GHz, we have designed an antenna at 28 GHz. The 28 GHz frequency is selected because this frequency has attracted significant attention for 5G applications. Hardware results for the 2.5 GHz antenna and the 28 GHz antenna are in accordance with the simulated results.

7.2 Future Work

Further research is underway to exploit the advantages of our proposed methodology. By increasing the number of arrays, we expect the overall gain of the antenna to increase. Subsequently, with a higher gain, we expect the proposed antenna to have applications in satellite communications. From above, it is evident that proposed hybrid beamforming methodology has immense potential for use in next-generation communication systems.

REFERENCES

[1] T. S. Rappaport, S. Sun, R. Mayzus, H. Zhao, Y. Azar, K. Wang, G. N. Wong, J. K. Schulz, M. Samimi, and F. Gutierrez. Millimeter wave mobile communications for 5g cellular: It will work! *IEEE Access*, 1:335–349, 2013.

[2] K Gyoda and Tatsuro Ohira. Design of electronically steerable passive array radiator (espar) antennas, 02 2000.

[3] N. Doose and P. A. Hoeher. On eirp control in downlink precoding for massive mimo arrays. In *WSA 2016; 20th International ITG Workshop on Smart Antennas*, pages 1–5, March 2016.

[4] G. Bochechka and V. Tikhvinskiy. Spectrum occupation and perspectives millimeter band utilization for 5g networks. In *Proceedings of the 2014 ITU kaleidoscope academic conference: Living in a converged world - Impossible without standards*, pages 69–72, June 2014.

[5] G. Brooker. Development of a w-band scanning conscan antenna based on the twist-reflector concept. In *ICMMT 2000. 2000 2nd International Conference on Microwave and Millimeter Wave Technology Proceedings (Cat. No.00EX364)*, pages 436–439, 2000.

[6] Y. A. Litinskaya, A. D. Nemshon, A. V. Stankovsky, S. V. Polenga, and Y. P. Salomatov. Experimental research of the antenna array with electronic and

combine electronic and mechanical beam steering. In *2016 International Siberian Conference on Control and Communications (SIBCON)*, pages 1–3, May 2016.

[7] Z. Ellahi and A. ur Rehman. Phased array antenna for the application of device free localization in indoor environments. In *2017 Intelligent Systems Conference (IntelliSys)*, pages 1074–1077, Sept 2017.

[8] K. Zarb-Adami, A. Faulkner, J. G. B. de Vaate, G. W. Kant, and P. Picard. Beamforming techniques for large-n aperture arrays. In *2010 IEEE International Symposium on Phased Array Systems and Technology*, pages 883–890, Oct 2010.

[9] S. Dutta, C. N. Barati, A. Dhananjay, and S. Rangan. 5g millimeter wave cellular system capacity with fully digital beamforming. In *2017 51st Asilomar Conference on Signals, Systems, and Computers*, pages 1224–1228, Oct 2017.

[10] X. Wu, D. Liu, and F. Yin. Hybrid beamforming for multi-user massive mimo systems. *IEEE Transactions on Communications*, pages 1–1, 2018.

[11] N. Kuga and H. Arai. A four beam-switched planar array antenna for mobile terminals. In *IEEE Antennas and Propagation Society International Symposium. 1995 Digest*, volume 3, pages 1450–1454 vol.3, June 1995.

[12] S. K. Karki, J. Ala-Laurinaho, V. Viikari, and R. Valkonen. Lens antenna design for e-band point-to-point radio links. In *2017 Progress In Electromagnetics Research Symposium - Spring (PIERS)*, pages 1625–1631, May 2017.

[13] W. J. Chen and J. P. Wang. Broadband dual-polarized high gain lens antenna array for base station applications. In *2017 IEEE International Symposium on*

Antennas and Propagation USNC/URSI National Radio Science Meeting, pages 827–828, July 2017.

[14] D. W. Jiang, Y. S. Zhang, H. Zhang, and J. Jin. A novel broadband reflect-array antenna with rectangle ring element for ku-band application. In *2012 IEEE MTT-S International Microwave Workshop Series on Millimeter Wave Wireless Technology and Applications*, pages 1–4, Sept 2012.

[15] I-Yu Chen, Chien-Jen Wang, Hua-Lin Guan, and C. F. Jou. Studies of suppression of the reflected wave and beam-scanning features of the antenna arrays. *IEEE Transactions on Antennas and Propagation*, 53(7):2220–2225, July 2005.

[16] Q. Han, V. Briend, and T. Ohira. Evaluation of the adaptive beamforming capability of an espar antenna using the genetic algorithm. In *2006 European Conference on Wireless Technology*, pages 59–62, Sept 2006.

[17] S. D. Assimonis, A. Theopoulos, and T. Samaras. A new high-gain and low-complexity pattern-reconfigurable antenna. In *2015 9th European Conference on Antennas and Propagation (EuCAP)*, pages 1–4, May 2015.

[18] L. Kulas. Simple 2-d direction-of-arrival estimation using an espar antenna. *IEEE Antennas and Wireless Propagation Letters*, 16:2513–2516, 2017.

[19] W. H. Jones and M. de La Chapelle. Connexion by boeingsm-broadband satellite communication system for mobile platforms. In *2001 MILCOM Proceedings Communications for Network-Centric Operations: Creating the Information Force*, volume 2, pages 755–758 vol.2, 2001.

[20] H. T. Liu, S. Gao, and T. H. Loh. Electrically Small and Low Cost Smart Antenna for Wireless Communication. *IEEE Transactions on Antennas and Propagation*, 60(3):1540–1549, March 2012.

[21] C.A. Balanis. *Antenna Theory: Analysis and Design*. Wiley, 2012.

[22] M.N.O. Sadiku. *Elements of Electromagnetics*. Oxford Series in Electrical an. Oxford University Press, 2018.

[23] K. Iigusa and T. Ohira. A simple and accurate mathematical model of electronically steerable parasitic array radiator antennas. In *First IEEE Consumer Communications and Networking Conference, 2004. CCNC 2004.*, pages 312–315, Jan 2004.

[24] Chen Sun, A. Hirata, T. Ohira, and N. C. Karmakar. Fast Beamforming of Electronically Steerable Parasitic Array Radiator Antennas: Theory and Experiment. *IEEE Transactions on Antennas and Propagation*, 52(7):1819–1832, July 2004.

[25] Shaafq Kausar, Hamood Ur Rahman, Tayyab Hassan, and Ahmed Kausar. Miniaturization of ESPAR Antenna Using Folded Monopoles and Conical Central Element. In *Radar, Antenna, Microwave, Electronics, and Telecommunications (ICRAMET), 2015 International Conference on*, pages 87–91. IEEE, 2015.

[26] K. Iigusa, K. Sato, and M. Fujise. A slim electronically steerable parasitic array radiator antenna. In *2006 6th International Conference on ITS Telecommunications*, pages 386–389, June 2006.

[27] T. Hassan, A. Kausar, H. Umair, and M. A. Anis. Gain Optimization of a Seven Element ESPAR Antenna Using Quasi-Newton Method. In *Microwave Technology Computational Electromagnetics (ICMTCE), 2011 IEEE International Conference on*, pages 293–296, May 2011.

[28] C. H. Papas and R. King. Input impedance of wide-angle conical antennas fed by a coaxial line. *Proceedings of the IRE*, 37(11):1269–1271, Nov 1949.

[29] Jun Ozawa, J. F. Cheng, and Yoichiro Watanabe. Adaptive beamforming of espar antenna with hamiltonian algorithm. 2009.

[30] R. Qian, M. Sellathurai, and D. Wilcox. A Study on MVDR Beamforming Applied to an (ESPAR) Antenna. *IEEE Signal Processing Letters*, 22(1):67–70, Jan 2015.

[31] T. H. Loh, H. Liu, and S. Gao. A cost-Effective Direct Magnitude Measurement Methodology for Smart Antennas. *IEEE Transactions on Antennas and Propagation*, 61(4):2043–2050, April 2013.

[32] Ahmed Umar Kausar, Farhan Aslam Khan, Tayyab Hassan, Adil Nasser, and Shafaq Kausar. Adaptive ESPAR Antenna System Modelling & Design. *International Journal of Simulation–Systems, Science & Technology*, 14(4), 2013.

[33] A. Pal, A. Mehta, D. Mirshekar-Syahkal, and H. Nakano. A Low-Profile Switched-Beam Dual-Band Capacitively Coupled Square Loop Antenna. In *Antennas and Propagation Conference (LAPC), 2013 Loughborough*, pages 563–566, Nov 2013.

[34] A. Mehta, D. Mirshekar-Syahkal, and P. J. Massey. Recent Progress in Switched Beam Single Element Antennas. In *Antennas and Propagation Conference, 2008. LAPC 2008. Loughborough*, pages 309–312, March 2008.

[35] L. Zhou, F. A. Khan, T. Ratnarajah, and C. B. Papadias. Achieving Arbitrary Signals Transmission Using a Single Radio Frequency Chain. *IEEE Transactions on Communications*, 63(12):4865–4878, Dec 2015.

[36] S. A. Mitilineos, K. S. Mougiakos, and S. C. A. Thomopoulos. Design and Optimization of ESPAR Antennas via Impedance Measurements and a Genetic Algorithm. *IEEE Antennas and Propagation Magazine*, 51(2):118–123, April 2009.

[37] M. Rzymowski, P. Woznica, and L. Kulas. Single-Anchor Indoor Localization Using ESPAR Antenna. *IEEE Antennas and Wireless Propagation Letters*, 15:1183–1186, 2016.

[38] R. Schlub, Junwei Lu, and T. Ohira. Seven Element Ground Skirt Monopole ESPAR Antenna Design from a Genetic Algorithm and the Finite Element Method. *IEEE Transactions on Antennas and Propagation*, 51(11):3033–3039, Nov 2003.

[39] J. H. Lee, J. S. Choi, and S. C. Kim. Cell coverage analysis of 28 ghz millimeter wave in urban microcell environment using 3-d ray tracing. *IEEE Transactions on Antennas and Propagation*, 66(3):1479–1487, March 2018.

[40] H. M. Rahim, C. Y. Leow, T. A. Rahman, A. Arsad, and M. A. Malek. Foliage attenuation measurement at millimeter wave frequencies in tropical vegetation.

In *2017 IEEE 13th Malaysia International Conference on Communications (MICC)*, pages 241–246, Nov 2017.

[41] W. A. Shittu, B. G. Bajoga, F. Anwar, and M. J. E. Salami. Prediction of received signal power and propagation path loss in open/rural environments using modified free-space loss and hata models. In *2008 IEEE International RF and Microwave Conference*, pages 126–130, Dec 2008.

[42] The Mathworks, Inc., Natick, Massachusetts. *MATLAB version 9.2.0.538062 (R2017a)*, 2017.

[43] K. Zeman, P. Masek, M. Stusek, J. Hosek, and P. Silhavy. Accuracy comparison of propagation models for mmwave communication in ns-3. In *2017 9th International Congress on Ultra Modern Telecommunications and Control Systems and Workshops (ICUMT)*, pages 334–340, Nov 2017.

[44] F. Vatalaro, G. E. Corazza, C. Caini, and C. Ferrarelli. Analysis of leo, meo, and geo global mobile satellite systems in the presence of interference and fading. *IEEE Journal on Selected Areas in Communications*, 13(2):291–300, Feb 1995.

[45] P. H. Wu. Geostationary Satellite Link Availability of Airborne Communication Codes. In *MILCOM 2005 - 2005 IEEE Military Communications Conference*, pages 2100–2106 Vol. 4, Oct 2005.

[46] M. A. Tyurin and R. V. Davidoff. Ku-band Airborne Satellite Communication Station. In *2007 17th International Crimean Conference - Microwave Telecommunication Technology*, pages 292–293, Sept 2007.

[47] D. Medina, F. Hoffmann, F. Rossetto, and C. H. Rokitansky. A Geographic Routing Strategy for North Atlantic In-Flight Internet Access Via Airborne Mesh Networking. *IEEE/ACM Transactions on Networking*, 20(4):1231–1244, Aug 2012.

[48] M. R. Anjum, M. A. Dida, P. Yin, W. Liu, and D. Yang. Design and Analyze the Airborne Satellite Communication Using Phased Array Antenna for Reliable Communications. In *5th IET International Conference on Wireless, Mobile and Multimedia Networks (ICWMMN 2013)*, pages 164–167, Nov 2013.

[49] T. Pultarova. Telecommunications - space tycoons go head to head over mega satellite network [news briefing]. *Engineering Technology*, 10(2):20–20, March 2015.

[50] O. Ceylan, A. Caglar, H. B. Tugrel, H. O. Cakar, A. O. Kislal, K. Kula, and H. B. Yagci. Small satellites rock a software-defined radio modem and ground station design for cube satellite communication. *IEEE Microwave Magazine*, 17(3):26–33, March 2016.